

TABLE I. Structure parameters for isomers of S_n^- , $n=2-4$, with energies ΔE relative to the ground state (eV). Bond lengths d_{ij} in a.u., bond angles α_i and dihedral angles γ_{ij} in degrees. Additional labels refer to the figures.

Molecule	Symmetry	State	ΔE
S_2^- $d_{12}=3.81$	$D_{\infty h}$	$^2\Pi_g$	0.0
S_3^- 1(a) $d_{12,13}=3.79$; $\alpha_1=115^\circ$	C_{2v}	2B_1	0.0
S_3^- 1(b) $d_{12,13}=4.17$; $d_{23}=4.20$; $\alpha_1=61^\circ$; $\alpha_{2,3}=60^\circ$	C_{2v}	2B_2	1.73
S_3^- 1(c) $d_{12,13}=4.06$	$D_{\infty h}$	$^2\Pi_u$	2.22
S_4^- 1(d) $d_{12,34}=3.71$; $d_{14}=5.83$; $d_{23}=4.28$; $\alpha_{1,4}=78^\circ$; $\alpha_{2,3}=102^\circ$	C_{2v}	2A_2	0.0
S_4^- 1(e) $d_{12,34}=3.69$; $d_{14,23}=4.92$	D_{2h}	2A_u	0.05
S_4^- 1(f) $d_{12,34}=3.76$; $d_{23}=4.03$; $\alpha_{2,3}=108^\circ$	C_{2h}	2B_g	0.13

TABLE II. Structure parameters for the isomers of S_5^- , with energies relative to the ground state (eV). Bond lengths d_{ij} in a.u., bond angles α_i and dihedral angles γ_{ij} in degrees. Additional labels refer to the figures.

Molecule	Symmetry	State	ΔE
S_5^- 2(a) $d_{12,45}=3.76$; $d_{15}=6.35$; $d_{23,34}=3.98$; $\alpha_{1,5}=87^\circ$; $\alpha_{2,4}=108^\circ$; $\alpha_3=95^\circ$; $\gamma_{12}, -\gamma_{45}=40^\circ$; $\gamma_{15}=0^\circ$; $\gamma_{23}, -\gamma_{34}=-76^\circ$	C_s	$^2A''$	0.0
S_5^- 2(b) $d_{12}=3.79$; $d_{23}=3.85$; $d_{34}=4.23$; $d_{45}=3.71$; $\alpha_2=111^\circ$; $\alpha_3=100^\circ$; $\alpha_4=105^\circ$; $\gamma_{23}=-62^\circ$; $\gamma_{34}=-11^\circ$	C_1	2A	0.04
S_5^- 2(c) $d_{12,45}=3.75$; $d_{23,34}=3.98$; $\alpha_{2,4}=112^\circ$; $\alpha_3=98^\circ$; $\gamma_{23,34}=-112^\circ$	C_2	2B	0.09

TABLE III. Structure parameters for isomers of S_6^- , with energies relative to the ground state (eV). Bond lengths d_{ij} in a.u., bond angles α_i and dihedral angles γ_{ij} in degrees. Additional labels refer to the figures.

Molecule	Symmetry	State	ΔE
S_6^- 2(e) $d_{12,56}=3.69$; $d_{23,45}=4.53$; $d_{34}=3.65$; $\alpha_{2,5}=99^\circ$; $\alpha_{3,4}=97^\circ$; $\gamma_{23,45}=-5^\circ$; $\gamma_{34}=-73^\circ$	C_2	2A	0.0
S_6^- 2(f) $d_{12,56}=3.80$; $d_{16}=5.09$; $d_{23,45}=3.96$; $d_{34}=3.98$; $\alpha_{1,6}=102^\circ$; $\alpha_{2,5}=107^\circ$; $\alpha_{3,4}=106^\circ$; $\gamma_{12,56}=64^\circ$; $\gamma_{16}=-62^\circ$; $\gamma_{23,45}=-76^\circ$; $\gamma_{34}=75^\circ$	C_2	2B	0.02
S_6^- 3(a) $d_{12}=4.97$; $d_{16,23}=3.80$; $d_{34,56}=3.81$; $d_{45}=4.71$; $\alpha_{1,2}=95^\circ$; $\alpha_{3,6}=112^\circ$; $\alpha_{4,5}=97^\circ$; $\gamma_{12,45}=0^\circ$; $\gamma_{16}, -\gamma_{23}=81^\circ$; $\gamma_{34}, -\gamma_{56}=82^\circ$	C_s	$^2A''$	0.10

TABLE IV. Structure parameters for isomers of S_7^- , with energies relative to the ground state (eV). Bond lengths d_{ij} in a.u., bond angles α_i and dihedral angles γ_{ij} in degrees. Additional labels refer to the figures.

Molecule	Symmetry	State	ΔE
S_7^- 3(f) $d_{12,67}=3.76$; $d_{17}=5.47$; $d_{23,56}=4.00$; $d_{34,45}=3.91$; $\alpha_{1,3,5,7}=107^\circ$; $\alpha_{2,6}=110^\circ$; $\alpha_4=109^\circ$; $\gamma_{12}, -\gamma_{67}=74^\circ$; $\gamma_{23}, -\gamma_{56}=-104^\circ$; $\gamma_{34}, -\gamma_{45}=82^\circ$	C_s	$^2A''$	0.0
S_7^- 4(a) $d_{12}=3.71$; $d_{17}=5.75$; $d_{23}=4.13$; $d_{34}=3.83$; $d_{45}=3.94$; $d_{56}=3.99$; $d_{67}=3.74$; $\alpha_1=100^\circ$; $\alpha_2=108^\circ$; $\alpha_3=103^\circ$; $\alpha_4=109^\circ$; $\alpha_5=104^\circ$; $\alpha_6=110^\circ$; $\alpha_7=93^\circ$; $\gamma_{12}=86^\circ$; $\gamma_{17}=-10^\circ$; $\gamma_{23}=-37^\circ$; $\gamma_{34}=-80^\circ$; $\gamma_{45}=70^\circ$; $\gamma_{56}=58^\circ$; $\gamma_{67}=-84^\circ$	C_1	2A	0.0

TABLE V. Structure parameters for isomers of S₈⁻, with energies relative to the ground state (eV). Bond lengths d_{ij} in a.u., bond angles α_i and dihedral angles γ_{ij} in degrees. Additional labels refer to the figures.

Molecule	Symmetry	State	ΔE
S ₈ ⁻ 5(a) $d_{12,56}=3.86$; $d_{18,45}=3.97$; $d_{23,67}=4.00$; $d_{34,78}=4.07$; $\alpha_{1,2,5,6}=109^\circ$; $\alpha_{3,4,7,8}=116^\circ$; $\gamma_{12,56}=-80^\circ$; $\gamma_{23,67}=94^\circ$; $\gamma_{18,45}=92^\circ$; $\gamma_{34,78}=-107^\circ$	D_2	2B_1	0.0
S ₈ ⁻ 5(b) $d_{23,67}=4.40$; $d_{12,34,56,78}=3.66$; $d_{18,45}=5.25$; $\alpha_{2,3,6,7}=101^\circ$; $\alpha_{1,4,5,8}=95^\circ$; $\gamma_{18,23,45,67}=0^\circ$; $\gamma_{12,56}$, $-\gamma_{34,78}=89^\circ$	C_{2v}	2B_1	0.06

charged and neutral systems. Examples are vertical detachment energies (VDE), the energy differences between the most stable isomer of the anion, and different states of the neutral cluster with the *ionic* structure, i.e., the ionization potentials (IP) of the anion. Since the stable structures of the neutral and charged clusters are generally different, the electron affinity (EA) of the neutral cluster—the energy gained when one electron is added to the most stable isomer—differs from the VDE of the anion. *All* of these energy differences require a calculation of the total energy for a charged system in a supercell geometry with periodic boundary conditions (PBC). The Coulomb energy per cell of a periodic array of charges diverges, and the potential zeros in charged and neutral systems must be determined consistently. We now describe how this is done and give further details of the calculations.

A. Total energy of charged states

We first carry out cluster calculations using PBC, but with an additional uniform charge to neutralize the system. This density is used to construct the Coulomb potential for an *isolated* cluster, subject to zero boundary conditions at infinity, by computing the Coulomb potentials for a series of periodic arrays in which the densities are separated by successively larger distances. It is reasonable to assume that the density between the cells is that of the uniform background, since the exact electronic density decays exponentially to zero outside an isolated cluster¹⁸ and should be negligible at the cell boundaries. In the limit of infinite separation, the background density vanishes everywhere and the Coulomb potential converges to the potential of the density without background charge subject to zero boundary conditions at

infinity (see the Appendix). The evaluation of the necessary integrals is performed in \mathbf{k} space using a “partial” FFT technique similar to that described in Ref. 19.

B. Computational details

As in an earlier application of this method to neutral clusters of sulfur,¹¹ we use the pseudopotential parameters of Bachelet *et al.*²⁰ with *sp* nonlocality. The calculations are performed in a large face-centered-cubic unit cell with lattice constant 30 a.u., but without any other symmetry restrictions. Routine checks ensure that the density is small near the cell boundaries, and the interaction between clusters in neighboring cells is minimized, if necessary, by moving the clusters rigidly. The calculations for the larger clusters were repeated using a larger cell (lattice constant 36 a.u.). As noted previously,¹¹ the bond lengths, bond angles, and dihedral angles change by less than $\sim 1\%$. As in earlier work on S₈ and related molecules (S₇O, S₇Se, Se₈, O₈),²¹ we have expanded the basis set of Ref. 11 to an energy cutoff for the orbital functions of 7 a.u. This corresponds to ~ 3200 plane waves [at $\mathbf{k}=0$], and the density was expanded in ~ 9000 plane waves.

Further tests involved increasing the FFT mesh from 32^3 to 48^3 points and the energy cutoff from 7.0 to 18.9 a.u., with an increase in the number of plane waves in the expansion of the density to over 39 000. The small change in the VDE of S⁻ (2.42 to 2.37 eV) indicates that further expansion of the basis set will change little. We have also tested the effect on our extrapolation scheme of increasing the dimensions of the unit cell. For the C₁ isomer of S₇⁻ discussed below [Fig. 4(a)], we increased the lattice constant from 30

TABLE VI. Structure parameters for isomers of S₉⁻, with energies relative to the ground state (eV). Bond lengths d_{ij} in a.u., bond angles α_i and dihedral angles γ_{ij} in degrees. Additional labels refer to the figures.

Molecule	Symmetry	State	ΔE
S ₉ ⁻ 6(a) $d_{12,89}=3.76$; $d_{19}=5.38$; $d_{23}=3.97$; $d_{34,56}=3.92$; $d_{45}=3.91$; $d_{67,78}=3.95$; $\alpha_{1,5,6,9}=109^\circ$; $\alpha_{2,4}=110^\circ$; $\alpha_3=105^\circ$; $\alpha_7=107^\circ$; $\alpha_8=112^\circ$; $\gamma_{12}=-77^\circ$; $\gamma_{19}=-55^\circ$; $\gamma_{23}=66^\circ$; $\gamma_{34}=84^\circ$; $\gamma_{45}=-78^\circ$; $\gamma_{56}=-75^\circ$; $\gamma_{67}=108^\circ$; $\gamma_{78}=-79^\circ$; $\gamma_{89}=105^\circ$	C_1	2A	0.0
S ₉ ⁻ 6(b) $d_{12,89}=3.71$; $d_{19}=5.72$; $d_{23,78}=4.09$; $d_{34,67}=3.84$; $d_{45,56}=3.95$; $\alpha_{1,9}=95^\circ$; $\alpha_{2,8}=108^\circ$; $\alpha_{3,7}=105^\circ$; $\alpha_{4,6}=111^\circ$; $\alpha_5=110^\circ$; γ_{12} , $-\gamma_{89}=112^\circ$; γ_{23} , $-\gamma_{78}=-35^\circ$; γ_{34} , $-\gamma_{67}=-95^\circ$; γ_{45} , $-\gamma_{56}=101^\circ$	C_s	${}^2A''$	0.06

to 36 a.u., enlarged the FFT mesh to 36^3 points and the number of plane waves in the expansion of the density to $\sim 16\,000$. The calculated VDE decreased by only 0.02 eV. The change in the energy of S^- using an extrapolation parameter of 16 instead of 8 (see the Appendix) was only $\sim 3 \times 10^{-5}$ eV, so that our choice of this parameter should be very reliable.

III. STRUCTURES OF THE ANIONS

In this section we present the structures of energetically low-lying isomers of sulfur cluster anions. Apart from the distances between the end atoms in the “broken ring” structures, we include in the figures and tables only interatomic distances shorter than 5.3 a.u., the minimum in the pair correlation function of liquid sulfur between the first peak for covalently bonded pairs and the second peak for nonbonded pairs.²² “Bonds” are shown black for distances < 4.8 a.u. and white from 4.8 to 5.3 a.u. The energy extrapolation has not been carried out self-consistently, so we have estimated the relative stabilities of *equally* charged clusters using self-consistent energies without extrapolation. There are few experimental data on the structure of sulfur cluster anions, and we compare our calculated geometries (Tables I–VI) with results for neutral clusters and other theoretical predictions where available. Distances and bond angles not given explicitly are related by symmetry to values in the tables. Angles are given to the nearest degree, and the sign of the dihedral angle γ has been chosen in accordance with the convention of Ref. 23.

A. S_2^-

The attachment of an additional electron to the neutral sulfur isomers generally leads to an appreciable increase in the bond lengths. The calculated value for S_2^- (see Table I) is $\sim 6\%$ larger than that in the neutral dimer (3.61 a.u.) and slightly larger than that reported below for S_3^- . In S_2^- the added electron occupies an antibonding $\pi_g^*(3p)$ orbital and the strength of the double bond in S_2 is reduced accordingly.

B. S_3^-

We have found three local minima in the energy surface for this ion (Table I). The open ground state [2B_1 , C_{2v} , Fig. 1(a)] differs from the C_{2v} singlet ground state of S_3 by having a ($\sim 3.6\%$) longer bond and a ($\sim 20\%$) smaller bond angle. The present values (see Tables I and VII) agree well with recent CI calculations (3.58 a.u., 117° for S_3 ; 3.76 a.u., 115° for S_3^-).¹⁵ The bond length in the matrix isolated anion has been estimated by electron paramagnetic resonance (EPR) to be 3.97 a.u.²⁴

The ground state valence electron configuration of the anion $1a_1^2 1b_2^2 2a_1^2 2b_2^2 3a_1^2 1b_1^2 1a_2^2 4a_1^2 3b_2^2 2b_1^1$ is the same as that described by other authors.¹⁵ The calculated dissociation energy (into S_2^- and S) is 4.4 eV/molecule (experimentally 3.3 eV/molecule),⁸ somewhat larger than the estimate found for the dissociation of S_3 .¹¹ The second C_{2v} structure [Fig. 1(b) and Table I] is a distortion of the D_{3h} structure (equilateral triangle) and has an energy much

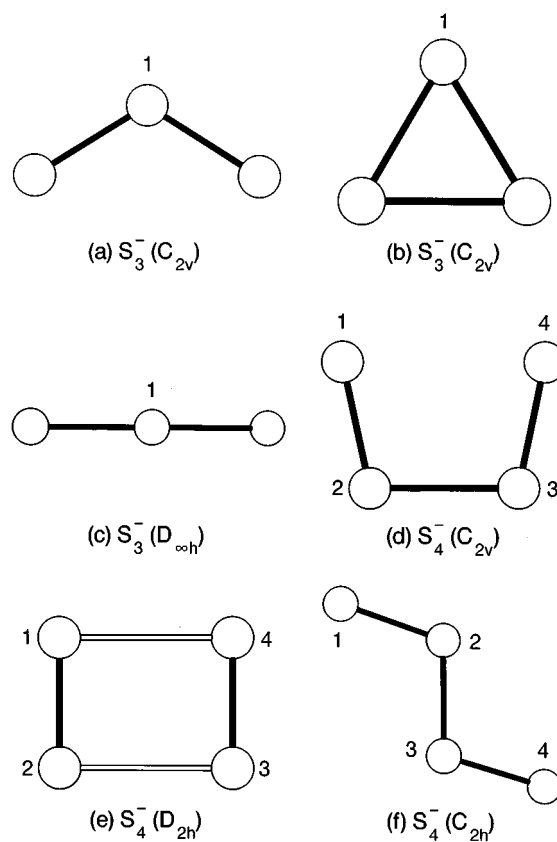


FIG. 1. Structures of (a)–(c) S_3^- and (d)–(f) S_4^- .

(1.73 eV) higher than the first and much longer bonds (4.20 a.u.). The structure of a high-lying linear [$D_{\infty h}$, Fig. 1(c)] isomer is also given in Table I.

C. S_4^-

Three structures of the anion [Figs. 1(d)–1(f)] have very similar energies (Table I). The most stable—a *cis*-planar structure with C_{2v} symmetry [Fig. 1(d)]—was also found in a recent theoretical study,¹⁵ with bond angles $\sim 12\%$ larger and the “long” bond distance $\sim 9\%$ smaller than ours.

We have noted that recent theoretical¹³ and experimental work⁴ on *neutral* S_4 indicate that the most stable isomer has *cis*-planar (C_{2v}) symmetry. This is supported by calculations using the present method, where we find that this isomer is 0.05 eV more stable than the planar rectangular ring structure [Fig. 1(e), D_{2h}] discussed previously.¹¹ The energy extrapolation scheme lifts the near-degeneracy between these two forms, the final separation being ~ 0.11 eV. The D_{2h} form of the anion is not stable, as the additional electron causes one of the longer bonds to open. A third structure 0.13 eV above the C_{2v} isomer is a planar *trans* isomer with C_{2h} symmetry [Fig. 1(f)]. A preference for the *cis* form is also evident in the larger anions. Other structures considered here—planar and nonplanar—had higher energies and were unstable on annealing at 300–500 K.

TABLE VII. Structure parameters for isomers of S_n, n=2,3,4,6,9 with energies relative to the ground state (eV). Bond lengths d_{ij} in a.u., bond angles α_i and dihedral angles γ_{ij} in degrees. Additional labels refer to the figures.

Molecule	Symmetry	ΔE
S ₂	D _{∞h}	0.0
d ₁₂ =3.61		
S ₃ 12(a)	C _{2v}	0.0
d _{12,23} =3.66; α ₂ =118°		
S ₃ 12(b)	D _{3h}	0.27
d _{12,23,13} =3.94; α _{1,2,3} =60°		
S ₄ 12(c)	C _{2v}	0.0
d _{12,34} =3.61; d ₂₃ =4.21; α _{2,3} =100°		
S ₄ 12(d)	D _{2h}	0.03
d _{12,34} =3.60; d _{14,23} =4.71; α _{1,2,3,4} =90°		
S ₄ 13(a)	C _{2h}	0.44
d ₁₂ =3.97; d _{13,24} =3.65; α _{1,2} =111°		
S ₆ 13(c)	D _{3d}	0.0
d _{12,...} =3.92; α _{1,...} =103°; γ _{23,16,45} =-γ _{12,34,56} =74°		
S ₆ 13(b)	D _{3h}	0.21
d _{14,25,36} =3.59; d _{12,...} =5.07; α _{123,...} =60°; α _{125,...} =90°		
S ₉ 13(d)	C ₂	0.0
d _{12,45} =3.88; d _{19,56} =3.94; d _{23,34} =3.92; d _{67,89} =3.90; d ₇₈ =3.91; α _{1,5} =107°; α _{2,4} =110°; α ₃ =103°; α _{9,6} =106°; α _{7,8} =109°; γ _{23,...} -γ ₄₅ =75°; γ _{12,...} -γ ₃₄ =-76°; γ _{19,56} =-63°; γ _{89,67} =113°; γ ₇₈ =-85°		

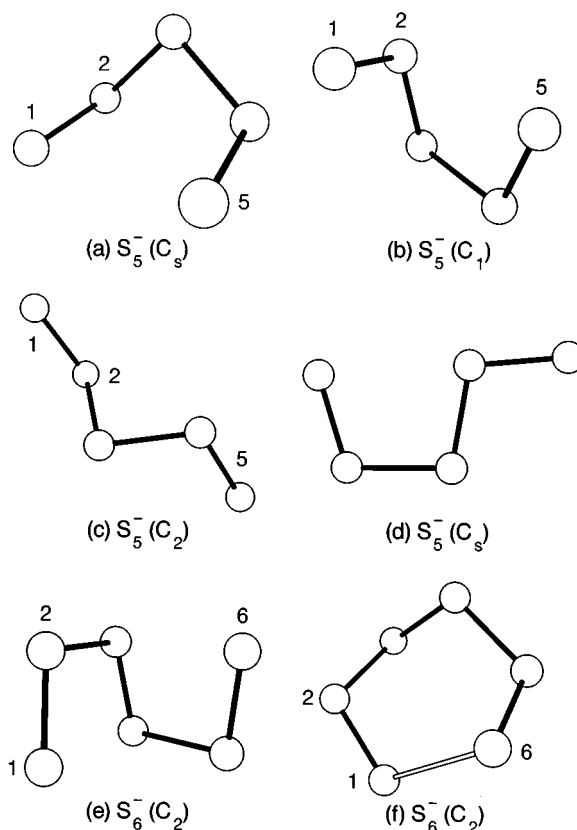
D. S₅⁻

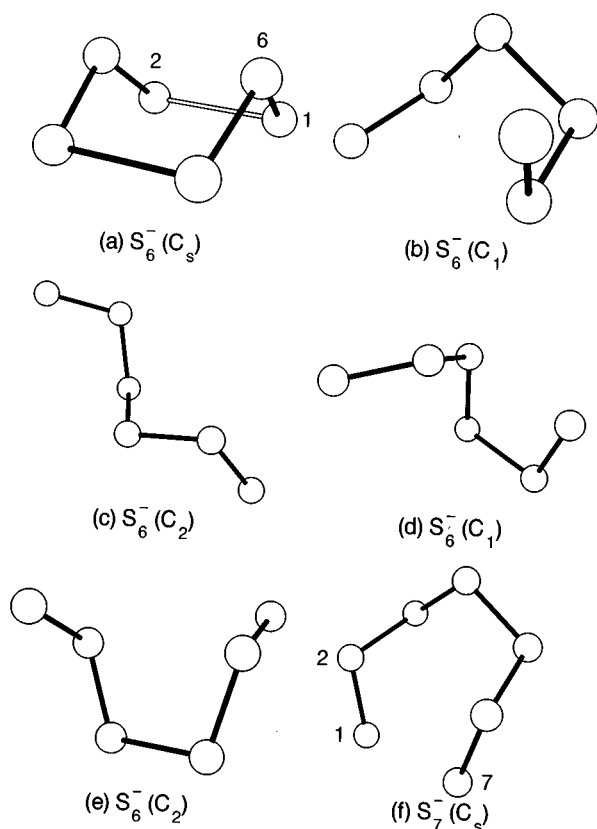
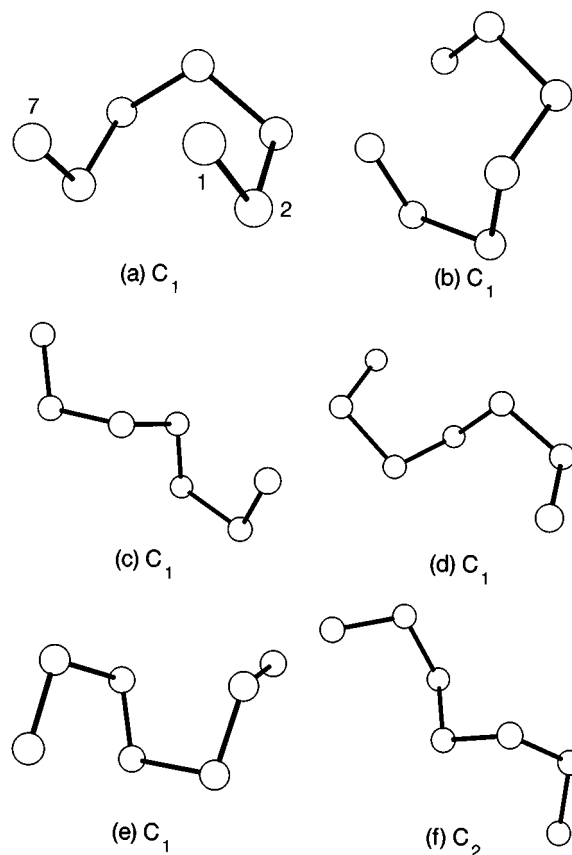
The most stable isomer in S₅⁻ (Table II) is a broken ring with C_s symmetry [Fig. 2(a)], reminiscent of the C_s “envelope” predicted for S₅,¹¹ with one bond broken by the additional electron. This has also been found in CI calculations of S₅⁻,¹⁵ where the large interatomic separation (5.70 a.u.) is 10% shorter than ours (6.35 a.u.). The extra electron occupies an antibonding orbital with a large amplitude in this region. We show below that the same is true for S₆⁻ and S₇⁻, where the addition of an electron to neutral rings also leads to bond breaking.

The next local minimum in the energy surface (0.04 eV higher) is a *cis-trans* (C₁) form [Fig. 2(b)]. The comparatively small dihedral angle in this cluster can be viewed as a remnant of the pattern already encountered in the *cis-planar* (C_{2v}) structure of S₄⁻. Another isomer (0.09 eV above the most stable) is a helical chain [Fig. 2(c)] with C₂ symmetry. The terminal bonds in this structure have a similar length to the bonds in S₃⁻, indicating a bond order between one and two. The central bonds are longer, approaching the value in catenapolysulfur S_∞ [3.90 a.u.].¹ A similar pattern is observed in the bond lengths of longer helical chains. A comparatively large gap of 0.18 eV separates these structures from a *cis-trans* planar (C_s) form [Fig. 2(d)]. This also contains the motif of the *cis-planar* (C_{2v}) isomer of S₄⁻ and was found by annealing the C_s isomer of neutral S₅ considered previously.¹²

E. S₆⁻

The structure of S₆⁻ [C₂, Fig. 2(e), Table III] was found by annealing a chainlike geometry and can be seen as two overlapping C_{2v} *cis-planar* sections. An alternative view as three weakly bound pairs is consistent with the change of the

FIG. 2. Structures of (a)–(d) S₅⁻ and (e)–(f) S₆⁻.

FIG. 3. Structures of (a)–(e) S_6^- and (f) S_7^- (C_s).FIG. 4. Structures of S_7^- .

bond length towards that of neutral S_2 (3.61 a.u.) as the center is approached. The dihedral angle (see Sec. III A) between the bisecting planes is $\sim 80^\circ$. A puckered chair-like S_6^- ring with C_2 symmetry [Fig. 2(f)] is only 0.02 eV higher in energy. The increase in the bond length (to 5.09 a.u.) caused by the additional electron is less than in the S_5^- ground state ring. The remaining structural parameters deviate little from the experimental values in S_6 ,¹ the bond lengths by at most 2%, the bond angles by less than 5%, and the dihedral angles by $\sim 2\%$.

Another C_2 boat structure [Fig. 3(a)], consisting of two weakly bound sulfur trimers, lies 0.10 eV above the isomer in Fig. 2(e). The energy minimum is shallow and the structure distorts readily to lower (C_1) symmetry on annealing. We also found a C_1 isomer [Fig. 3(b)], a helical (C_2) chain [Fig. 3(c)], and two structures containing the *cis*-planar motif of S_4^- [Figs. 3(d) and 3(e)], with energies 0.12, 0.17, 0.20, and 0.25 eV above the most stable isomer. The all-*trans* chain [Fig. 3(c)] is slightly less stable (by 0.05 eV) than the *cis*-*trans* chain [Fig. 3(b)], illustrating the trend to favor compact geometries. Annealing of an all-*cis* chain also led to the puckered ring [Fig. 2(f)]. The last two isomers show both chain segments and a planar tetramer. Similar forms are observed in S_7^- and S_8^- .

F. S_7^-

As in the case of S_5^- , there are no structures consisting entirely of planar sections, and the most stable isomer is a

distortion of the neutral S_7 ground state, a chair-like ring with C_s symmetry.^{25,26} The “long” bond in S_7 (experimentally 4.12 a.u.) opens to give a distorted chair-like C_s form [Fig. 3(f) and Table IV] with a broken bond of length 5.47 a.u. This structure was found by annealing an all-*cis* chain. The other changes in the structure of S_7 are also small, with bond lengths changing by less than $\sim 1\%$, and angles by less than $\sim 5\%$. The second longest bond of the S_7 chair (experimentally 3.97 a.u.) can also open in the anion, leading to another C_1 isomer [Fig. 4(b)] only 0.02 eV less stable than the first. The additional charge is localized on a bond of length 5.59 a.u.

Another isomer that is almost degenerate with Fig. 3(f) is a distorted boat (C_1) structure [Fig. 4(a)] derived from a C_s isomer in neutral S_7 (Ref. 11) by breaking its longest bond. Other isomers [Figs 4(c)–4(e)] show the planar sections familiar from the *cis*-planar (C_{2v}) structure of S_4^- and have energies in a narrow range (0.02 eV wide) starting 0.28 eV above the ground state. A helical (C_2) chain [Fig. 4(f)] lies 0.36 eV above the most stable isomer. Hybrids of planar and chain-like sections tend to become more stable than helices as the cluster size increases.

G. S_8^-

The best known of the neutral sulfur clusters is the D_{4d} crown-shaped ring,^{27,28} and our calculations indicate that the most stable S_8^- isomer is a distortion of this structure

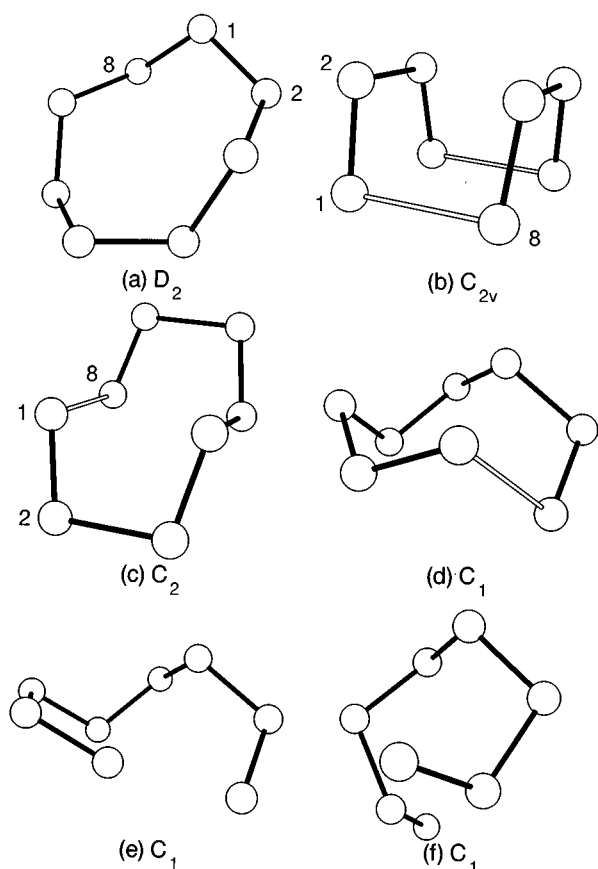


FIG. 5. Structures of S_8^- . (a)–(d) “Closed,” (e)–(f) “open.”

to D_2 symmetry [Fig. 5(a)]. Compared with the experimental data for (neutral) orthorhombic (α -) S_8 at 100 K,²⁹ the additional electron induces an approximately uniaxial stretch, with two bonds on opposite sides of the ring increasing in length by 5%.

A C_{2v} isomer [Fig. 5(b)] is only 0.06 eV higher in energy than the ring. It may be viewed as two loosely bound *cis*-planar (C_{2v}) tetramers, such as found in S_4^- , since the bond lengths (Table V) deviate by only $\sim 3\%$ from those in S_4^- , and the orbitals along the shortest distance (5.25 a.u.) between the tetramers are weakly bonding. Since the LSD approximation often overestimates the strengths of bonds between closed shell systems,³⁰ the long, weak bond between the tetramers may be an artifact of this approximation.

The *cis*-planar tetramer is found as a structural unit in other isomers. For example, a C_2 structure with slight distortions from C_{2h} symmetry [Fig. 5(c)] lies 0.34 eV above the ground state and differs from Fig. 5(b) only in the relative orientation of the planar segments. An isomer with C_1 symmetry and a planar section [Fig. 5(e)] lies 0.02 eV the C_2 structure. Two others with terminal planar sections, including one with C_2 symmetry and planar units at each end, lie a further 0.07–0.08 eV higher.

In addition to the most stable all-*cis* ring isomer [Fig. 5(a)], we considered a ring derived from it by inverting two dihedral angles. The energy of the resulting C_1 species [Fig. 5(d)] is 0.35 eV above that of the ground state ring. This

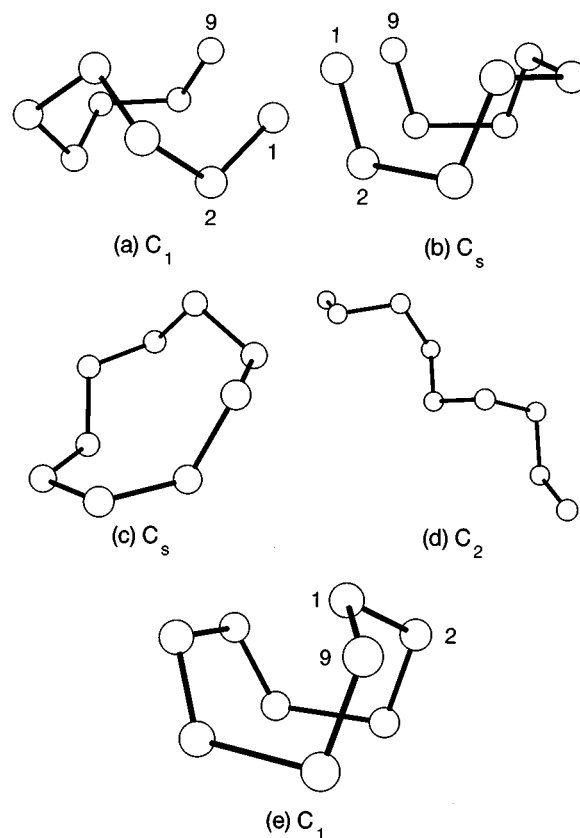


FIG. 6. Structures of S_9^- .

structure is more compact than that in Fig. 5(a), and the increased strain caused by the additional electron results in one weak bond of length 5.19 a.u.

There are numerous chain structures derived by the addition of a single atom to S_7^- chains. The lengths of the central bonds of the all-*trans* helical chain (0.56 eV) are close to the measured values in catenapolysulfur (S_∞ , 3.90 a.u.),¹ the bond and dihedral angles are $\sim 3\%$ larger and $\sim 10\%$ smaller, respectively. Several chain-like structures differ from the helix in the sign of one or more dihedral angles and have energies within 0.20 eV. Of particular interest are structures with one and two terminal planar tetramers (C_1 and C_2 symmetry, respectively) that are 0.12 eV more stable than the helical chain.

H. S_9^-

The rapidly increasing number of isomers with cluster size rules out any attempt at completeness for larger clusters, but we have studied several isomers of S_9^- to see whether trends in the smaller anions continue. The experimental geometries of S_9 and its ions are not known,³¹ but the theoretical prediction^{11,12} of a C_2 ring as the most stable form of S_9 is consistent with the Raman spectra of microcrystalline samples.³¹ The corresponding structure obtained with the present basis set is given in Table VII. The most stable isomer of S_9^- encountered is a C_1 distortion of the neutral ground state [Fig. 6(a) and Table VI], where one interatomic

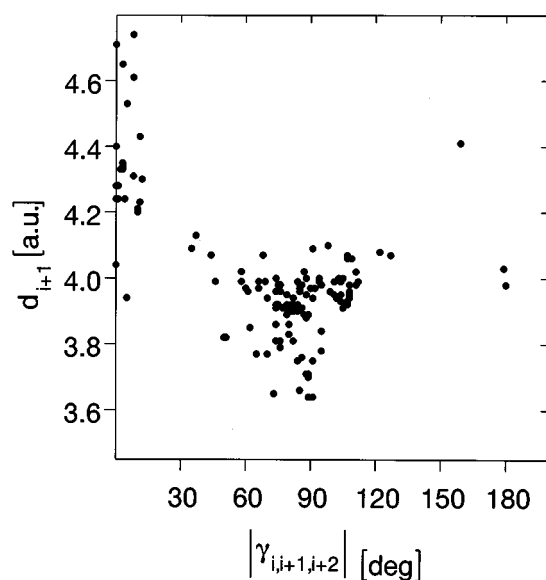


FIG. 7. Variation of the length of the central bond d of three adjacent bonds with dihedral angle γ .

separation increases from 3.94 to 5.38 a.u. and can no longer be viewed as a bond. The anion structure related to the C_s boat isomer of S_9 [Fig. 6(b)] lies 0.06 eV higher. It also has C_s symmetry, and can be derived from the S_8^- isomer [Fig. 5(b)] by inserting a single atom in place of one of its longest bonds. The *cis*-planar (C_{2v}) tetramers are distorted, the dihedral angle being 35° .

A C_s chair isomer [Fig. 6(c)] is 0.10 eV higher in energy, with structural parameters similar to those reported previously for an isomer of S_9 .¹¹ The all-*trans* helical chain [Fig. 6(d), C_2] lies 0.40 eV above the ground state and has a pattern of bond lengths and angles that is similar to that found in the helical isomer of S_8^- . As in the case of the smaller clusters, isomers with one (C_1) and two (C_2) terminal planar tetramers are more stable than the helix, in S_9^- by 0.02 and 0.12 eV, respectively. The energy of the last structure that we considered, a C_1 cage [Fig. 6(e)] very similar to a C_s isomer of S_9 described in Ref. 11, was 0.14 eV above the helix. The additional electron causes the longer bonds between the atoms labeled 3,4 and 7,8 in Fig. 6(e) to increase to 4.61 and 4.74 a.u., respectively, significantly larger than the longest bond in the *cis*-planar (C_{2v}) tetramer unit (~ 4.28 a.u.).

I. Trends

1. Structures

The planar C_{2v} motif first encountered in S_4^- also appears in planar sections of the larger anions. Structures consisting entirely of this pattern exist only for even values of n , in which case they are among the most stable isomers. This motif represents a compromise between a relatively open structure that can accommodate an additional charge and a closed structure with one large internuclear separation (of average length 5.77 a.u.). Its presence is apparent in Fig. 7, which plots bond length against dihedral angle γ for all an-

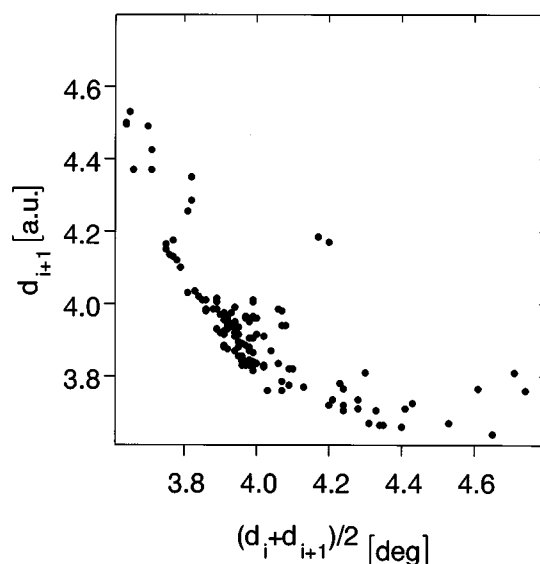


FIG. 8. Variation of bond length d with the mean length of the two neighboring bonds.

ion structures shown in the tables. A similar relationship has been observed by Steudel and co-workers^{27,28,32-34} for neutral sulfur clusters. Apart from a peak near 90° reminiscent of the “normal” dihedral angle distribution,³⁵ there is a second cluster of values near $\gamma=0^\circ$. The elongation of the central bond as γ decreases from 90° to 0° is favorable for a negatively charged molecule. A second trend noted by Steudel and co-workers for the neutral clusters is the inverse relationship between bond length and the mean of the lengths of the neighboring bonds. This trend is also found in the anionic structures (Fig. 8, for all anion structures shown in the tables).

Another family of anion geometries of low energy consists of the opened or puckered rings of the neutral clusters, where at least one of the bonds is strained or broken due to the presence of the additional electron. The ground states of S_5^- , S_7^- , S_8^- , and S_9^- belong to this family.

Open chain-like structures without planar sections also occur, and their stability relative to the most stable isomers decreases with increasing cluster size. Hybrids of all-*trans* chains with the C_{2v} *cis*-planar unit of S_4^- occur in S_6^- – S_8^- and are on average ~ 0.1 eV more stable than their all-*trans* counterparts.

2. Binding energies

The calculated binding energies per atom,

$$E_b^-/n = [(n-1)E_1 + E_1^- - E_n^-],$$

are plotted in Fig. 9 for all anionic structures shown in the tables. The stability increases with increasing cluster size n , so that S_n^- clusters should be observable for all n in the range studied here. With the exceptions of the upper C_{2v} and $D_{\infty h}$ isomers of S_3^- , there are numerous minima in the potential energy surface of the anion clusters with similar energies.

The second energy differences

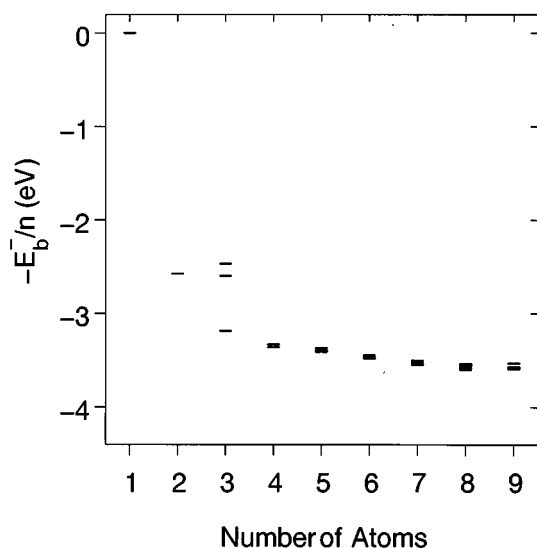


FIG. 9. Binding energies per atom E_b^-/n for S_n^- clusters as a function of n .

$$\Delta^2 E_n^- = E_{n+1}^- + E_{n-1}^- - 2E_n^-$$

are shown in Fig. 10 for the most stable isomers. This quantity is useful in discussing the relative abundances of clusters,^{36,37} as it indicates the difference between the fragmentation energies for the processes $S_{n+1}^- \rightarrow S_n^- + S$ and $S_n^- \rightarrow S_{n-1}^- + S$. The small negative values at S_5^- and S_7^- indicate that these clusters should be less stable than the neighboring anions, whereas the large positive values for S_2^- and S_3^- suggest a relatively high abundance.

3. Vertical detachment energies

The calculations of the VDE can be illustrated by considering the atom ($n=1$), where the energies of the anion S^- and the multiplet structure of the neutral atom must be evaluated. We use the fitting procedure of von Barth³⁸ to

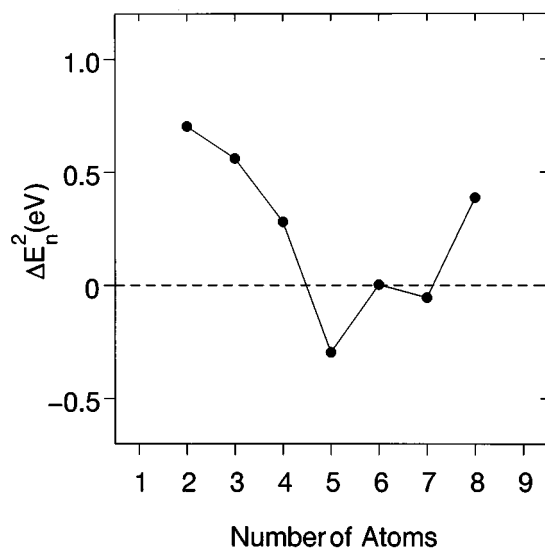


FIG. 10. Second energy differences $\Delta^2 E_n^-$ for the S_n^- clusters as a function of n .

solve an (overdetermined) set of linear equations relating the multiplet energies to the calculated energies of single determinantal states.³⁹ In the case of sulfur, or for any atom with the valence configuration p^2 or p^4 , the energies for the multiplet 3P , 1D , and 1S can be obtained by fits to the corresponding equations. The limits on the reliability of the procedure are shown by the results for the (single determinant) state 3P , where a direct calculation gives a VDE of 2.42 eV. A fit using all three determinants gives 2.21 eV, while the measured value is 2.08 eV.^{6,40}

The spin multiplets of the neutral clusters with the ground state geometries of all ions from S_2^- to S_9^- were obtained using the above procedure, and tables of the results are obtainable from the authors.⁴¹ It should be noted that the DF formalism applies to the lowest state of a given symmetry and not just to the ground state of a given molecule. A comparison of calculated and measured VDE is a central part of the present study, and full details are given in Sec. VI.

In Fig. 11 we plot the VDE values for the cage- and ring-like structures found for the anions. For $n > 5$ there is a variety of chain structures, and the ranges of VDE values are shown by bars for $n=6-8$. The differences between the VDE of the two classes of structures is striking. Apart from a small peak at S_5^- , the broken ring structures show almost constant or even decreasing VDE with increasing cluster size, while the values for the chains increase at first and then saturate near S_6^- . The outermost electron is more tightly bound in the chains, an effect that has also been observed in carbon clusters.⁴²

The eigenvalue spectra support this view, since there is a relatively small gap between the uppermost two occupied orbitals in the chain isomers. Since the sum of the eigenvalues is one contribution to the total energy, a small gap leads to a high VDE. The gap decreases continuously with increasing cluster size from 0.83 eV in the C_{2h} chain isomer of S_4^- to 0.06 eV in the C_2 helical chain isomer of S_9^- . A

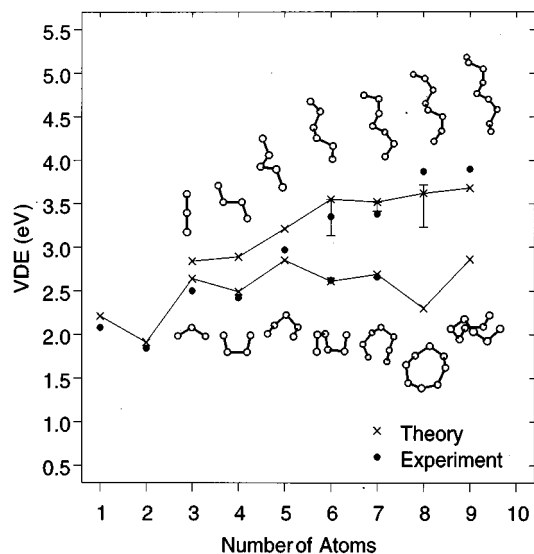


FIG. 11. Vertical detachment energies of sulfur anions S_n^- , $n=1-9$. Circles: experiment, crosses: calculations, including values for helical chains. The bars cover the values for other chain structures.

TABLE VIII. Calculated vibration frequencies (ω_e , cm⁻¹) of selected isomers of neutral S_n, n=2,3,4,6,9. Additional labels refer to the figures.

Molecule	Symmetry	Method	Frequency ω_e
S ₂	$D_{\infty h}$ ($^3\Sigma_g^-$)	Expt. ^a	725.65 (σ_g)
		Expt. ^b	725 ± 12
		here	691 (σ_g)
		CI ^c	778 (σ_g)
S ₃ 12(a)	C_{2v} (1A_1)	Expt. ^d	256 (a_1), 575 (a_1), 656 (b_2)
		here	247 (a_1), 583 (a_1), 660 (b_2)
		DF ^e	257 (a_1), 602 (a_1), 690 (b_2)
		MP2 ^f	263 (a_1), 577 (a_1), 758 (b_2)
S ₃ 12(b)	D_{3h}	here	478 (e'), 625 (a'_1)
		DF ^g	478 (e'), 619 (a'_1)
S ₄ 12(c)	C_{2v} (1A_1)	here	111 (a_1), 238 (a_2), 334 (b_2), 336 (a_1), 652 (b_2), 689 (a_1)
		CI ^h	141 (a_1), 222 (a_2), 353 (b_2), 421 (a_1), 693 (b_2), 701 (a_1)
S ₄ 12(d)	D_{2h} (1A_g)	here	67 (b_{3u}), 249 (a_u), 322 (a_g), 335 (b_{1g}), 668 (b_{2u}), 697 (a_g)
		CI ⁱ	120i (b_{2u}), 262 (a_u), 334 (a_g), 355 (b_{3g}), 782 (b_{1u}), 877 (a_g)
S ₄ 13(a)	C_{2h} (1A_g)	here	98 (a_u), 107 (b_u), 216 (a_g), 462 (a_g), 638 (b_u), 648 (a_g)
		CI ^j	101 (a_u), 140 (b_u), 252 (a_g), 528 (a_g), 678 (a_g), 681 (b_u)
S ₆ 13(b)	D_{3h}	here	108 (e''), 161 (a''_2), 207 (e'), 249 (a''_1), 271 (a'_1), 301 (e''), 672 (e'), 710 (a'_1)
S ₆ 13(c)	D_{3d}	Expt. ^k	180 (e_u), 203 (e_g), 265 (a_{1g}), 312 (a_{2u}), 390 (a_{1u}), 451 (e_u), 462 (e_g), 477 (a_{1g})
		here	160 (e_u), 187 (e_g), 255 (a_{1g}), 303 (a_{2u}), 347 (a_{1u}), 458 (e_u), 474 (e_g), 476 (a_{1g})
S ₉ 13(d)	C_2	Expt. ^l	100, 104, 111, 117, 151, 155, 161, 181, 188, 215, 222, 245, 256, 297, 416, 436, 442, 454, 455, 463, 477
		here	89 (a), 119 (b), 135 (b), 148 (a), 170 (a), 201 (b), 219 (b), 230 (a), 230 (b), 242 (b), 295 (a), 393 (a), 419 (a), 429 (a), 435 (b), 454 (a), 465 (a), 483 (a)

^aReference 55.^bPresent work, photoelectron detachment.^cReference 13, CISD(TZ2P+f).^dReference 59.^eReference 62, TZ2P+f, LSD.^fReference 61, quoted by Ref. 62, MP2, 6-31G*.^gReference 62, TZ2P+f, LSD.^hReference 13, CISD(DZP).ⁱReference 13, CISD(DZP).^jReference 13, CISD(DZP).^kReference 72.^l α -S₉ from Ref. 31.

detailed study of the densities shows that the additional electron occupies an antibonding orbital localized mainly on the terminal bonds of the chain. The potential energy is then lower in longer chains with larger distances between the ends. This picture is consistent with the saturation of the VDE found in longer chains.

The charged broken rings and planar structures are more compact, and both the energy of the highest occupied electron state and its separation from the next occupied orbital

TABLE IX. Calculated vibration frequencies (ω_e , cm⁻¹) of S₂⁻ and S₃⁻.

Molecule	Symmetry		ω_e
S ₂ ⁻	$D_{\infty h}$, $^2\Pi_g$	Expt. ^a here	589.4 (σ_g) 577
S ₃ ⁻ 1(a)	C_{2v} , 2B_1	Expt. ^b here	235.5 (a_1), 535 (a_1), 571 (b_1) 216 (a_1), 529 (a_1), 557 (b_1)

^aReference 54 (S₂⁻ in ultramarine green).^bReference 54 (from blue and red sulfur solutions in dimethylformamide and hexamethylphosphoramide).

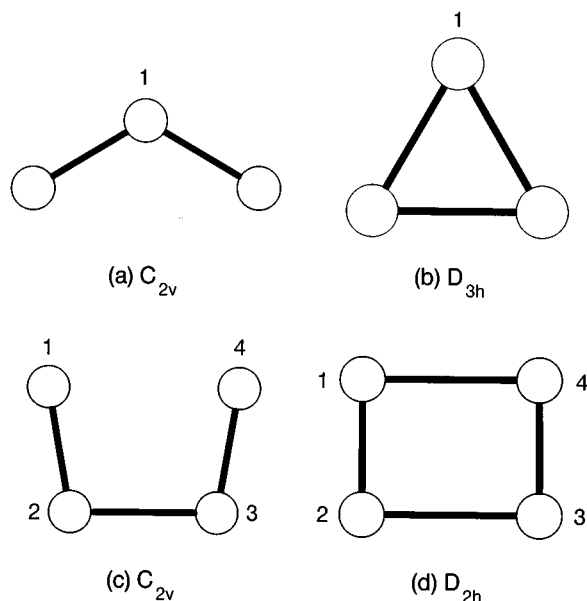
remain large as the cluster size increases. Apart from S₁⁻, S₂⁻ and the D_{3h} and D_{2h} rings of S₃⁻ and S₄⁻, the largest eigenvalue gap (2.23 eV) and the lowest VDE was found in the first genuine ring in S₈⁻. The exceptionally low VDE of S₂⁻ is not surprising, since the additional electron must occupy an antibonding orbital with a relatively large amplitude.

IV. VIBRATION FREQUENCIES

Recent experimental developments have made it possible to measure vibration frequencies and electron excitations simultaneously, and spectra showing resolved vibrational features have been reported for numerous clusters in the gas phase (see Refs. 43–48, and references therein). In a typical measurement,^{49,50} a mass-selected beam of cluster anions is produced and the kinetic energy spectrum of photo-detached electrons is measured. High-resolution spectra contain information about the electronic and vibrational states of the neutral cluster, as it is a consequence of the Franck–Condon principle that transitions occur from the ground state of the anion to the vibrationally excited states of the neutral cluster.

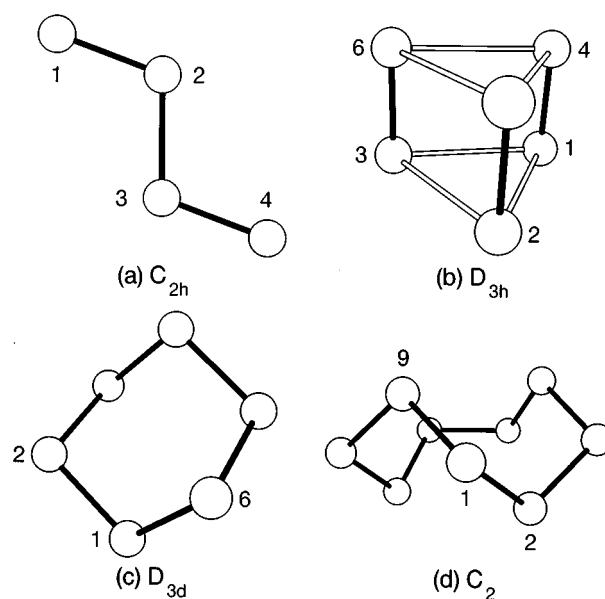
We have used an eigenmode detection scheme⁵¹ based on the self-consistent multiple-signal classification (MUSIC) procedure described by Kohanoff⁵² to calculate the vibration frequencies of the neutral clusters closest to the geometry of the most stable isomer of the anion. The calculations require non-thermally-equilibrated MD trajectories for the system in question. We remove an electron from the anion and allow the systems to evolve in MD runs (at 300–500 K) to find the closest minimum on the energy surface of the neutral cluster. The cluster atoms are then displaced by small amounts, either randomly or according to the eigenvectors of the expected normal modes, and the trajectories followed for 2000 to 5000 time steps at 300 K. The results for selected clusters are given in Table VIII, together with experimental frequencies. The measured frequencies of S₂⁻ and S₃⁻ (Table IX) are for solutions. The dependence on the host is shown, e.g., by the Raman frequencies of S₂⁻ in Na I, K I, and Rb I (599.8, 600.0, and 605.7 cm⁻¹, respectively).⁵³ Data for S₂⁻ and S₃⁻ in other solvents⁵⁴ are given in Table IX. The calculated frequency for S₂ (691 cm⁻¹) underestimates the experimental value⁵⁵ by less than 5%.

The structures of both S₃⁻ isomers [Figs. 1(a) and 1(c)] relax on ionization to the C_{2v} isomer of S₃ [Fig. 12(a)], whose structural parameters are given in Table VII. Meyer

FIG. 12. Structures of selected isomers of neutral S_3 and S_4 .

*et al.*⁵⁶ assigned a band in the gas phase absorption spectrum at 590 cm^{-1} to the a_1 stretching frequency. Raman bands at 651 and 585 cm^{-1} for S_3 in an SO_2 matrix and at 662 and 583 cm^{-1} in solid argon⁵⁷ were assigned to the b_2 and a_1 stretching modes.⁵⁸ A Raman study of sulfur vapor⁵⁹ identified three fundamental modes at 656 , 575 , and 256 cm^{-1} , and a more detailed investigation by the same group assigned the a_1 bending and stretching modes to wave numbers of 281 and 581 cm^{-1} , respectively.⁶⁰ In the infrared spectra in solid argon, the b_2 stretching mode has been identified,⁴ although the wave numbers reported (674.5 , 676.2 , and 680 cm^{-1}) depend on the trapping site. While there is some scatter in the measured frequencies, our calculated values of the harmonic vibration frequencies are in overall agreement and deviate least (less than 4%) from the results in Ref. 59. The reoptimization after ionization of the C_{2v} structure [Fig. 1(b)] of S_3^- gave the D_{3h} isomer of S_3 [Fig. 12(b), Table VII], to which no measured spectral features have been attributed. Vibration frequencies calculated for these two isomers of S_3 using other methods^{61,62} are also given in Table VII.

The fundamental vibration modes of S_4 have been studied in both Raman and infrared spectroscopy. Clark and Cobbold⁵⁴ reported Raman bands at 352 and 674 cm^{-1} , and Brabson *et al.*⁴ measured infrared spectra of sulfur in an argon matrix. Absorptions at 661.6 and 642.4 cm^{-1} behaved differently on annealing and photolysis, and were identified with the C_{2v} open chain [Fig. 12(c)] and the branched ring nonplanar isomers of S_4 , respectively. The vibration frequencies found in the present investigation are compared with those of Quench *et al.*¹³ in Table VIII. While it is not possible to make a definite assignment of the basis of the calculated frequencies, particularly as the measured values are in a matrix, our calculations show modes at 652 and 689 cm^{-1} for the C_{2v} isomer [Fig. 12(c)]. In Table VIII we also

FIG. 13. Structures of selected isomers of neutral S_4 , S_6 , and S_9 .

present the calculated vibration frequencies in the D_{2h} [Fig. 12(d)] and C_{2h} isomers [Fig. 13(a)] of S_4 .

The S_6^- structure [Fig. 2(e)] relaxes to the prismane (D_{3h}) form of the neutral cluster [Fig. 13(b)] after ionization. If the structure [Fig. 2(f)] is taken as the starting geometry for S_6 , it relaxes to the (D_{3d}) ground state [Fig. 13(c)]. The vibration frequencies calculated for both S_6 structures are given in Table VIII together with measured values of the latter.

The vibration frequencies in S_9 are of particular interest. Although two different forms have been identified, it has not yet proved possible to prepare single crystal samples.³¹ The essential details of the structure could nevertheless be determined from the Raman spectra, since the distribution of the vibration frequencies was quite different from those of other sulfur rings. In particular, there were gaps in the frequency distributions between 310 and 410 and 490 and 600 cm^{-1} . The frequency spectrum was only consistent with C_1 or C_2 symmetry, and with relatively narrow ranges of bond lengths (3.84 – 3.95 a.u.) and dihedral angles (70° – 130°).

We have performed a detailed study of the vibration frequencies of the most stable isomer found in the MD/DF calculations,¹¹ and compare the results with the measured Raman frequencies³¹ in Table VIII. The low symmetry of the molecule and the relatively large number of modes (21) complicate the calculations, and we include only modes whose symmetries can be identified unambiguously. The differences between the frequencies in the α and β forms of S_9 (Ref. 31)—the symmetric ring deformation, e.g., leads to intense Raman lines at 188 and 181 cm^{-1} , respectively—indicate that we cannot expect detailed agreement between theory and experiment. Nevertheless, the overall agreement is satisfactory, particularly concerning the frequency gaps mentioned above. We have little doubt that the most stable isomer in S_9 is the C_2 structure shown in Fig. 13(d).

V. EXPERIMENT

The general features of the apparatus have been described in detail elsewhere,⁶³ and we devote the present section to a discussion of those aspects specific to the present work on sulfur.

A. Experimental setup

1. Cluster ion source

The sulfur clusters are generated in a pulsed arc cluster ion source (PACIS).⁶⁴ The negative electrode is a vertical molybdenum rod of diameter 10 mm, and the reservoir is a 9 mm hole drilled 10 mm into the top. Molten sulfur is poured into the reservoir and allowed to harden. The positive electrode is a 5 mm tungsten rod mounted above the reservoir, and the gap between the tip of the upper electrode and the rim of the reservoir is maintained at ~ 2 mm during cluster generation. The reservoir allows two to three days of stable operation.

A pulse of He gas is flushed through the gap between the two electrodes during ignition of the arc, which is achieved by applying a high voltage (600 V) across the electrodes. An electric discharge burns with a current limited to 10 A and triggers the low voltage/high current arc. The voltage of the arc power supply can be adjusted between 0–450 V, and the total resistance of the arc circuit is constant ($\sim 0.05 \Omega$). Ignition of the arc requires a minimum voltage of about 40 V and a current of 800 A, and the ignition time can be varied continuously between 10 and 500 μ s. The repetition rate is limited by the detachment laser (see below) to 20 Hz. While the amount of neutral vaporized material is roughly proportional to the electric energy (the product of the ignition time and the arc voltage), the peak intensity of negative ions is greatest with a pulse length of 20 μ s and a voltage of 80–300 V, corresponding to a current of 1600–6000 A. As the amount of material in the reservoir decreases, the voltage must be increased to obtain optimum anion intensities.

The arc burns between the two molybdenum electrodes, but neither metal atoms nor other significant impurities have been found in the mass spectrum of the negative ions. This is surprising, since sulfur is an insulator, and the rim of the reservoir may function as a “candle wick” to vaporize some sulfur with each pulse. An intense signal of molybdenum cluster anions is observed if the reservoir contains no sulfur.

The He pulse carries the vaporized material into a 5 cm long channel of diameter 4 mm, where the He/sulphur plasma cools and sulphur clusters grow. These clusters then enter a 5 cm long conical nozzle and are cooled further in a supersonic jet. After passing a skimmer, the negatively charged clusters are accelerated in a pulsed electric field (Wiley–McLaren time-of-flight mass spectrometer).

The resulting mass spectrum depends on the following parameters of the source:

- (1) the intensity of the He gas pulse (stagnation pressure);
- (2) the time delay HA between the opening of the He valve and the ignition of the arc;
- (3) the time delay AE between ignition and the switching on of the electric field;

- (4) the voltage of the arc; and
- (5) the duration of the arc.

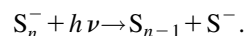
It is important to discuss the effect of changing these parameters, since this can result in the preferential generation of different isomers. A lower intensity of the He pulse results in a slower transport of the clusters through the extender and favors the formation of larger clusters. The time delay HA has a similar influence, because at the beginning and the end of the He pulse its intensity and therefore its flow velocity is low. The parameter AE determines whether clusters leaving the source first or later are detected in the mass spectrum. Clusters leaving the source immediately after ignition have spent a short time in the extender and are smaller. The voltage of the arc determines the rate of vaporization and the partial pressure of S, a large value of which results in more collisions and larger clusters. The duration of the arc has only a minor influence on the mass spectrum.

The effects of changing the above parameters are not independent, so it is difficult to obtain a complete understanding of the growth processes in the source. Nevertheless, the most important parameter appears to be the time spent by the clusters in the extender. It has been found for carbon clusters⁶⁵ that a very long extender at low He gas flow favors isomers with highly symmetric geometries (i.e., those that need time to form), while a short extender at high flow favors low symmetry isomers that form rapidly.

2. Electron spectrometer

The anion beam is separated, according to their velocities, into a sequence of bunches of clusters with a defined mass. The beam is directed through the source region of a “magnetic bottle”-type time-of-flight electron spectrometer. A selected bunch is irradiated by a UV-laser pulse, the detached electrons are guided by magnetic fields towards the detector, and their kinetic energy determined from the measured time of flight. A photoelectron spectrum is the plot of measured electron intensity against binding energy BE (photon energy minus kinetic energy).

Two photon energies are used in the present experiment: 3.49 and 4.66 eV corresponding to the third and fourth harmonics of a Nd–Yag laser, respectively. The laser flux—about 100 mJ cm^{-2} —is high enough to allow fragmentation to take place via multiphoton processes, and features of the spectrum of S^- were found in the spectra of several S_n^- clusters. These result from the process



A second photon can detach the electron from the monomer, resulting in a superposition of the spectra of the monomer and the cluster. The relative intensities of these features in the spectra vary, since this process depends nonlinearly on the laser flux, which may vary during the measurements. In all cases, however, these peaks are relatively small and easy to identify.

The energy resolution of the spectrometer depends on the kinetic energy of the electrons and the velocity of the anions. It is limited here to 40–70 MeV by charging arising

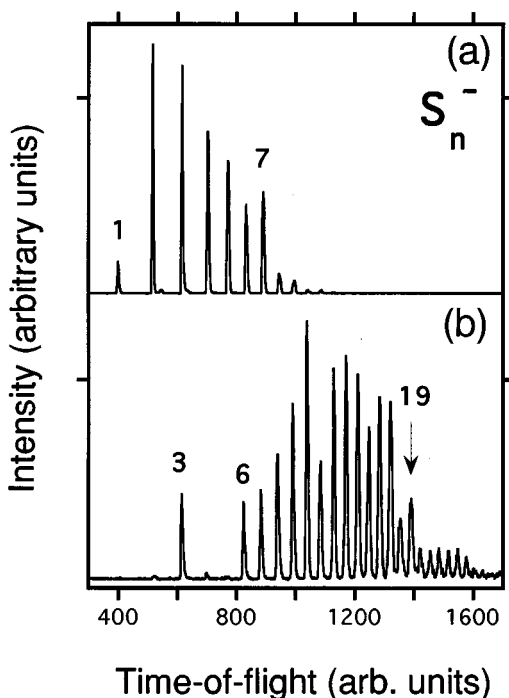


FIG. 14. Mass spectra of S_n^- clusters generated by the PACIS. (a) Slow cooling of the sulfur plasma, (b) more rapid cooling. The larger average size in the latter is due to the higher concentration of S in the carrier gas.

from reactions between sulfur and the surfaces of the optic elements. There is an additional uncertainty in the absolute value of the BE of ± 0.05 eV.

B. Results

1. Mass spectra

Figure 14 displays the comparison of two mass spectra of S_n^- clusters obtained at two different adjustments of the PACIS. In case *a* the source is adjusted to favor small clusters with $n=2-7$. The intensity is low for the monomer, highest for the dimer, and then decreases slightly up to $n=6$. The intensity of S_7^- is again slightly higher and then there is a sharp drop for the larger clusters. With the exception of the trimer, clusters with $n < 6$ have a very low intensity in spectrum *b*. The progression starts at S_6^- and reaches a maximum at S_{10}^- . Only S_3^- , S_6^- , and S_7^- have relatively high intensities in both spectra.

It is also possible to generate mass spectra with an intensity distribution averaged between the two spectra shown, for the monomer alone, or for very large clusters. The two spectra displayed in Fig. 14 are of special interest, because the photoelectron spectra for S_6^- and S_7^- differ completely, indicating the generation of different isomers with different source adjustments. Since all the adjustment parameters differ in the two cases and each spectrum can be obtained using more than one set of parameters, it is difficult to analyze the growth processes responsible. However, spectrum *a* is probably the result of a slower process similar to an annealing of the clusters, and spectrum *b* the result of a more rapid cooling process.

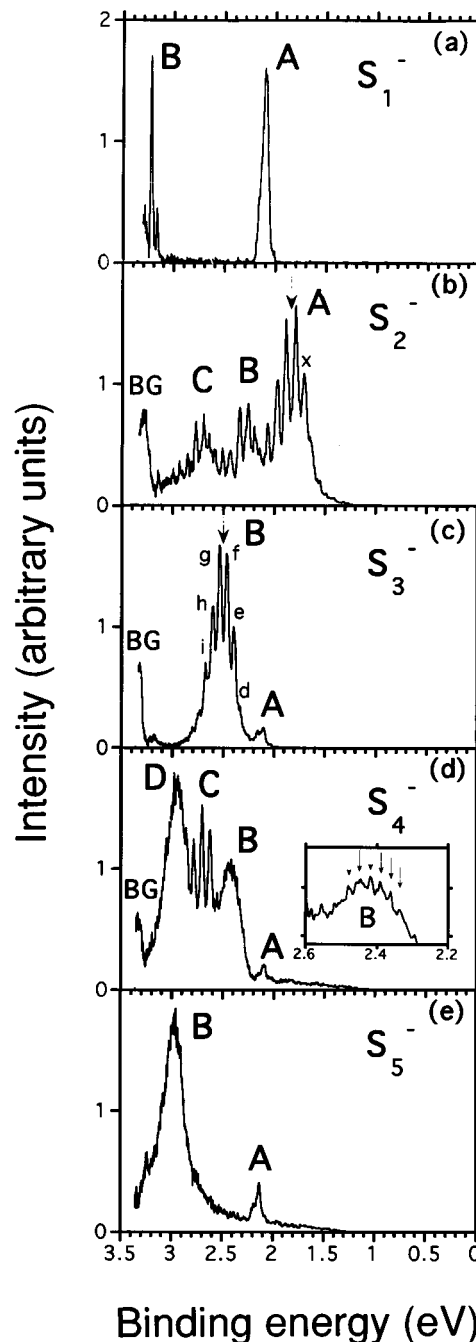


FIG. 15. Photoelectron spectra of S_n^- clusters ($n=1-5$) recorded at $h\nu=3.49$ eV photon energy. See the text for a discussion of the features marked.

The acceleration of the anions in the time-of-flight mass spectrometer is collinear with the supersonic jet. The jet velocity, which must be added to the velocity resulting from the electric field, depends on the stagnation pressure of the expansion and leads to slight shifts in the peak positions in the mass spectra. In spectrum *b*, e.g., the He pulse is more intense, the clusters have shorter times of flight than in *a* and spend less time in the extender. If all other parameters were the same, the average cluster size would be smaller in *b* than in *a*. However, using a higher arc voltage increases the rate

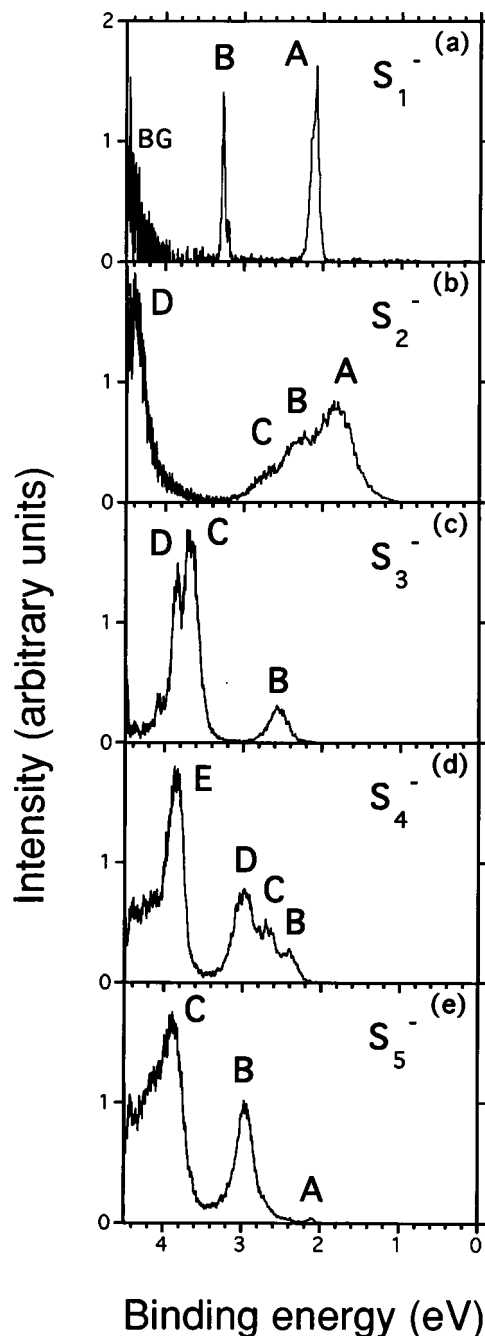


FIG. 16. Photoelectron spectra of S_n^- clusters ($n=1-5$) recorded at $h\nu=4.66$ eV photon energy. See the text for a discussion of the features marked.

of vaporization and the partial pressure of sulfur, and larger clusters can result.

2. Photoelectron spectra

Figures 15–18 display photoelectron spectra of the S_n^- clusters recorded at photon energies $h\nu$ of 3.49 (Fig. 15) and 4.66 eV. The VDE and the emission threshold can be determined from these spectra. The VDE is taken as the BE of the maximum of the peak corresponding to the transition from the electronic ground state of the anion into the electronic ground state of the neutral cluster. An unambiguous determi-

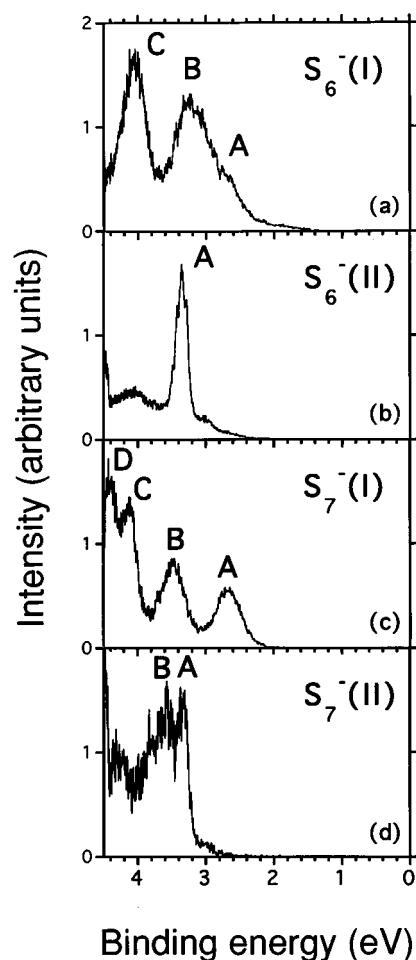


FIG. 17. Photoelectron spectra of S_6^- and S_7^- recorded at $h\nu=4.66$ eV photon energy. Spectra are shown for each cluster for two source adjustments corresponding to the mass spectra shown in Fig. 14. Adjustment (a) S_6^- (I) and S_7^- (I), adjustment (b) S_6^- (II) and S_7^- (II).

nation of this maximum is not possible in larger clusters with several states close to the ground state of the neutral cluster (Fig. 17). The VDE is estimated in such cases from the leveling of the emission signal at higher BE after the initial increase. Where this occurs, we increase the BE by 0.2 eV to allow for the estimated full width at half-maximum (FWHM) of the unresolved peak.

The emission threshold is determined by fitting a linear slope to the onset of the emission signal at lowest BE. The onset is taken as the intersection of this line with the base line. In some spectra we observe an exponential threshold behavior, which develops gradually into a linear increase at higher BE. The exponential tail may correspond to hot bands and is neglected in the determination of the onset.

Vibrational fine structure is resolved for S_n^- with $n=2,3,4,6$, corresponding to transitions from the ground state of the anions. The vibration frequencies are assigned to modes of states of the neutral cluster. For S_4^- a second progression is found for a transition into an excited state of S_4 . The VDE, emission thresholds, and frequencies are listed in Table X and the binding energies corresponding to

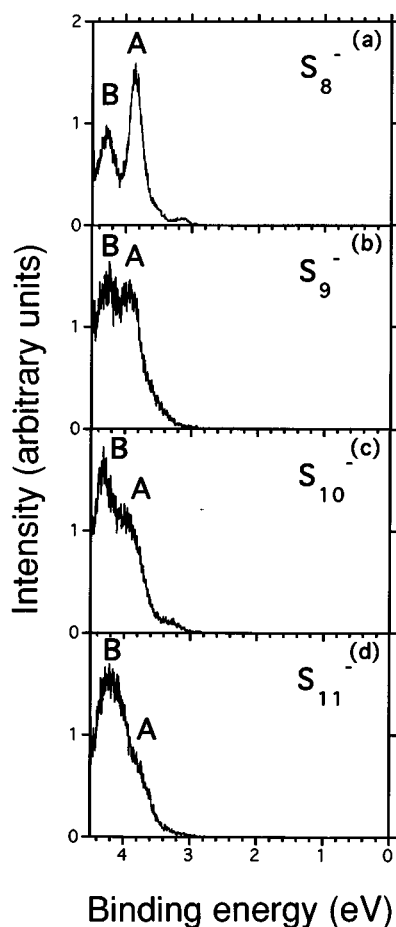


FIG. 18. Photoelectron spectra of S_n^- clusters ($n=8-11$) recorded at $h\nu=4.66$ eV photon energy. See the text for a discussion of the features marked.

different transitions in Table XI. We discuss the spectra for the individual clusters in the remainder of this section.

3. S₁⁻

Feature A in the spectra of S₁⁻ [Figs. 15(a) and 16(a)] is assigned to the transition from the electronic ground state of

TABLE X. S_n^- clusters: vertical detachment energies (VDE, eV), emission thresholds (eV), and vibration frequencies of S_n (cm^{-1}), with uncertainties in brackets. Calculated VDE are also given. There are many chain-like isomers. Values in square brackets are for helical chains.

n	VDE		Thrush	ν_1	ν_2
	Expt.	Calc.			
2	1.84 (0.05)	1.91	1.565 (0.05)	725 (12)	
3	2.50 (0.05)	2.64	2.31 (0.1)	570 (24)	
4	2.42 (0.05)	2.49	2.22 (0.03)	250 (16)	630 (24)
5	2.97 (0.03)	2.85	2.80 (0.05)		
6(I)	2.62 (0.1)	2.61	2.26 (0.1)		
6(II)	3.35 (0.05)	[3.55]	3.21 (0.07)	570 (32)	
7(I)	2.66 (0.05)	2.69	2.26 (0.05)		
7(II)	3.38 (0.05)	[3.52]	3.16 (0.05)		
8	3.87 (0.07)	[3.62]	3.59 (0.05)		
9	3.90 (0.1)	[3.68]	3.6 (0.1)		
10	3.90 (0.15)		3.5 (0.1)		
11	3.75 (0.2)		3.43 (0.1)		

the anion to the ground state of the sulphur atom (3P_2). The multiplet fine structure with a splitting of 71 MeV (Ref. 66) is not resolved. The BE of feature A corresponds to the electron affinity of S (2.077 eV),⁶ and B is assigned to the transition into the 1D state of neutral S (3.223 eV BE=2.077 eV electron affinity plus 1.146 eV excitation energy). The spectrum recorded at $h\nu=4.66$ eV [Fig. 16(a)] shows a feature at very low kinetic energy (4.4–4.5 eV BE, denoted BG) that corresponds to background electrons. These are generated by scattered light striking surfaces within the spectrometer and are observed in several spectra (denoted BG in each case).

4. S₂⁻

The spectra of S₂⁻ [Figs. 15(b) and 16(b)] are in good agreement with earlier work of Celotta *et al.*⁷ Feature A is assigned to the transition between the ground states of S₂⁻ and S₂, and a single vibrational progression with a frequency of 725 ± 12 cm^{-1} (Table X) is assigned to the latter. The VDE, corresponding to the maximum of feature A, is 1.84 ± 0.05 eV (arrow, see Table X) and the onset is at 1.565 ± 0.05 eV. In Ref. 7, the adiabatic electron affinity was given as 1.663 ± 0.04 eV (position of the 0–0 transition).

TABLE XI. Binding energies (at the maxima) of transitions in the photoelectron spectra of S_n^- (eV). Assignments A–D correspond to those in the spectra (Figs. 15–18), experimental numbers are given in the left column with uncertainties in brackets, calculated values in the right column. “Frag” denotes features assigned to photoemission from S₁⁻ ions generated by photofragmentation.

n	A		B		C		D		E						
2	1.84	(0.05)	1.91	2.3	(0.1)	2.45	2.73	(0.1)	2.98	4.4	(0.15)				
3	Frag			2.50	(0.05)	2.64	3.7	(0.1)	3.73/3.77	3.9	(0.1)	3.95			
4	Frag			2.42	(0.05)	2.49	2.7	(0.1)		2.96	(0.05)	3.19	3.87	(0.1)	3.96
5	Frag			2.97	(0.03)	2.85/3.28	3.9	(0.1)	3.81/3.92						
6(I)	2.62	(0.1)	2.61	3.3	(0.15)	3.17	4.1	(0.1)	3.80						
6(II)	3.35	(0.05)	3.55												
7(I)	2.66	(0.05)	2.69	3.47	(0.07)	3.88	4.14	(0.07)	4.15	4.4	(0.1)	4.51			
7(II)	3.38	(0.05)	3.52	3.6	(0.2)	3.62									
8	3.87	(0.07)	3.62/3.89	4.3	(0.07)	4.12									
9	3.9	(0.1)	3.68/3.94	4.3	(0.1)	4.24									
10	3.9	(0.15)		4.35	(0.1)										
11	3.75	(0.2)		4.1	(0.15)										

These authors assigned the 0–0 transition to the first well resolved vibrational transition at low BE [X in Fig. 15(b)], which is at 1.709 ± 0.015 eV in our spectrum. The difference between the measured positions of the 0–0 transition (1.663 and 1.709 eV) in the two measurements indicates the experimental uncertainties present. The differences between the VDE, the emission threshold, and EA show that they are by no means identical.

Features B and C, which have vibrational fine structures very similar to that in A, correspond to transitions into electronically excited states of S_2 (see Table XI). The spectrum recorded at $h\nu=4.66$ eV shows a feature with binding energy 4.3 eV [D in Fig. 16(b), Table XI] that is also assigned to a transition into an excited state of the dimer. It is located at almost the same BE as the background. The intensity of the dimer emission signal is much higher than the background signal, so that we may neglect the contribution of the background.

5. S_3^-

The spectrum of S_3^- recorded at $h\nu=3.49$ eV [Fig. 15(c)] shows a feature (A) that we assign to emission from the monomer as a result of fragmentation (see Sec. V A 2). Feature B is assigned to the ground state transition in accord with earlier measurements.⁸ The VDE is 2.50 ± 0.05 eV and the emission threshold 2.31 ± 0.1 eV. The position of the first well resolved vibrational transition [Fig. 15(c)] at lowest BE is 2.396 ± 0.02 eV, in analogy to the dimer, and a similar vibrational progression was found in the earlier work. However, the onset (BE of the 0–0 transition= 2.106 ± 0.014 eV) and the intensity maximum (VDE= 2.41 ± 0.03 eV) are shifted significantly towards lower BE, suggesting a different vibrational temperature of the anions. Another possibility is a reduced transmission of the hemispherical analyzer for electrons with low kinetic energies. Since the photon energy in the earlier experiment was relatively low ($h\nu=2.707$ eV) and the minimum pass energy was about 0.2 eV, the complete Franck–Condon profile of this transition could not be recorded.

The vibration frequency we find (570 ± 24 cm^{-1}) is larger than that in Ref. 8 (500 ± 48 cm^{-1}). A reevaluation of the earlier data yields a spacing between the first four observed transitions [denoted a–d, a–c not observed in Fig. 15(c)] of 500 cm^{-1} and a larger spacing of 550 cm^{-1} between features d–f. The measured position of feature g at the low energy cutoff might be shifted towards lower BE due to the decreasing transmission. Our analysis is based on the spacing between features e–i (h and i were not observed in the earlier work). If feature d is assigned to the 0–0 transition, the difference in the vibration frequency might be due to the difference between hot and cold bands. The earlier work indicates that the BE of feature d is 2.302 ± 0.07 eV, which corresponds to the weak transition near the first well resolved peak [e in Fig. 15(c)] on the low BE side. Accordingly, either feature d (BE= 2.326 eV) or feature e (BE= 2.396 eV) in our spectrum could be assigned to the 0–0 transition. Two transitions into excited states of the neutral trimer are observed in the spectrum recorded at $h\nu=4.66$ eV (C and D, see Table XI).

6. S_4^-

The spectrum of S_4^- recorded at $h\nu=3.49$ eV [Fig. 15(d)] shows a feature (A) that we assign to emission from the monomer as a result of fragmentation (see above). Feature B [Figs. 15(d) and 16(d)] is assigned to the ground state transition. The VDE is 2.42 ± 0.05 eV and the emission threshold is 2.22 ± 0.03 eV. Feature B exhibits a vibrational fine structure corresponding to a frequency of 250 ± 16 cm^{-1} (see insert). A second feature (C), with a much more pronounced vibrational progression corresponding to a vibration frequency of 630 ± 24 cm^{-1} , is observed with BE 2.7 eV. Two other features (D and E) correspond to transitions into higher excited states of S_4 .

7. S_5^-

Feature A [Figs. 15(e) and 16(e)] is assigned to fragmentation into S_1^- (see Sec. V A 2), and B to the ground state transition with a VDE of 2.97 ± 0.03 eV and an emission threshold of 2.80 ± 0.05 eV. Another feature (C) arises from a transition into an excited state and is observed in the spectrum recorded at $h\nu=4.66$ eV [Fig. 16(e), Table XI]. No vibrational fine structure has been resolved.

8. S_6^-

Two different photoelectron spectra [Figs. 17(a) and 17(b)] have been recorded for S_6^- using the source adjustments *a* and *b* shown in the mass spectra of Fig. 14. We have also found source parameters that produce a superposition of the two photoelectron spectra shown. Indeed, the smooth, relatively weak emission signals in the BE range from 2.4–4.4 eV observed in Figs. 17(b) and 17(a) are almost identical. We assign the dominant features (A, B, and C) in the spectra [Figs. 17(a) and 17(b)] to photoemission from two different isomers of S_6^- , which we denote (I) and (II), respectively.

It was not possible to generate pure S_6^- (II), so that Fig. 17(b) includes a contribution from the spectrum of S_6^- (I). The only vibrational fine structure observed, feature A in the spectrum of S_6^- (II), corresponds to a frequency of 570 ± 32 cm^{-1} (Table X).

9. S_7^-

As in the case of S_6^- , two different spectra [Figs. 17(c) and 17(d)] have been recorded for S_7^- , corresponding to two different isomers: S_7^- (I) and S_7^- (II). The latter was more difficult to generate and the photoelectron spectrum exhibits a rather poor signal-to-noise ratio. Fortunately, the contribution from S_7^- (I) to this spectrum is very small. No vibrational fine structure has been resolved.

10. $S_8^- - S_{11}^-$

Figure 18 displays the photoelectron spectra of the larger S_n^- clusters up to $n=11$. These clusters have relatively high VDE and show at most two clearly resolved transitions at relatively high BE. The origin of the weak features in the spectra of S_8^- and S_{10}^- at lower BE (3.0–3.4 eV) is unclear. For S_n^- with $n=9-11$ we observe a single feature that con-

sists of two peaks (A and B) with relatively broad, overlapping Franck–Condon distributions, and we determine the positions of the peak maxima by fitting. No vibrational fine structure could be resolved in the spectra of these species.

VI. COMPARISON OF THEORY AND EXPERIMENT

The experimental results presented in Sec. V will now be compared with the results of the calculations described in Secs. III and IV. We shall discuss the VDE, the adiabatic electron affinities, the vibrational frequencies, and the relative stabilities of the isomers.

A. Vertical detachment energies

Figure 11 shows a comparison of the calculated VDE with values extracted from the photoelectron spectra, including values for S₆⁻ and S₇⁻ found in both spectra. More details are given in Tables X and XI. The calculated values are shown for the most stable closed and open isomers. In the case of ions with $n > 5$, there is a variety of chain structures and we show both the range of VDE values and the result for the helical chain.

The overall agreement is remarkably good. For the clusters up to S₅⁻ the experimental VDE agree with the values for the most stable closed structures to within 0.15 eV, and the two measured values for S₆⁻ and S₇⁻ are very close to the calculated VDE of the most stable closed and open forms. The experimental values for S₈⁻ and S₉⁻ are in the same range as those for the chain-like structures. For the cases where a definite assignment of the transition could be made, the largest discrepancy was in the C_{2v} (ground) state of S₃⁻, where the calculated and measured VDE were 2.64 and 2.50 ± 0.05 eV, respectively.

The VDE plotted in Fig. 11 are for transitions to the most stable state in the neutral clusters. However, transitions into excited states of S_{*n*} can be identified and provide valuable additional information. A comparison of some of the measured peak positions in the photoelectron spectra with calculated excitation energies is given in Table XI. In the dimer, e.g., the first three peaks (1.84, 2.45, and 2.73 eV) are in satisfactory agreement with the excitation energies to the ³Σ_g⁻, ¹Δ_g, and ¹Σ_g⁺ states of S₂ (1.91, 2.45, and 2.98 eV). Energy differences in larger clusters can provide structural information. For S₃⁻, the measured excitation energies (2.50, 3.7, and 3.9 eV) are consistent with transitions for the open structure [Fig. 1(a)] to the ¹A₁, ³A₂/³B₁, and ³B₂ states of the neutral cluster (2.64, 3.73/3.77, and 3.95 eV), but not with excitations for the ring structure [Fig. 1(b)] (1.34, 2.93, and 2.94 eV for the ¹A₁, ³A₂, and ³B₁ states, respectively). The measured binding energies in S₄⁻ (Table XI) are consistent with the calculated multiplet structures of the C_{2v} [Fig. 1(d)] and D_{2h} [Fig. 1(e)] geometries, but incompatible with the results for the C_{2h} form [Fig. 1(f)] (2.89, 3.36, and 4.07 eV for ¹A_g, ³B_u, and ¹B_u, respectively). As noted above, tables of the multiplet structures calculated for other sulfur cluster anions are obtainable from the authors.⁴¹

B. Adiabatic electron affinities

The adiabatic electron affinity is the energy difference between the optimized structures of anion and neutral cluster. The largest discrepancy between calculation and experiment was found for the C_{2v} ground state of S₃⁻, where the calculated value (2.50 eV) is larger than the experimental (2.396 ± 0.02 eV). The calculated value for the C_{2v} isomer of S₄⁻ (2.38 eV) agrees very well with the results of a CI calculation with Davidson correction, 2.46 eV.¹⁵ The comparatively small theoretical AEA for S₆⁻ (1.68 eV) reflects the large difference between the structures of the ground states of the anion (C₂) and the neutral ring cluster (D_{3d}).

C. Vibration frequencies

The calculated vibration frequencies were compared with earlier data in Sec. IV. In two- and three-atom clusters (Tables VIII and IX) the agreement is generally better than found with other methods of calculation. For S₄, the measured frequencies correspond better with calculated values for the C_{2v} and D_{2h} isomers than with the C_{2h} form, as might be anticipated from the relative stabilities calculated for the three structures.

The only frequency measured for the S₆ structure (570 ± 32 cm⁻¹) is significantly higher than both the calculated and Raman frequencies of the D_{3d} isomer and falls in a pronounced gap of the spectrum for the D_{3h} isomer. Since the vibrational structure was only observed in spectrum S₆⁻ (II), where the anions are chain-like, this is evidence that the neutral cluster does not have time to relax to one of the more stable isomers during the measurement. It is also consistent with the observation³ that *all* unbranched sulfur rings regardless of the size have no fundamental frequencies above 530 cm⁻¹. To examine this point further, we have studied the vibrations of S₆ with the helical (C₂) geometry found for the S₆⁻ anion. The existence of a totally symmetric (*a*) vibration with frequency 619 cm⁻¹ provides further support for the above picture.

VII. DISCUSSION AND CONCLUDING REMARKS

We have performed a detailed study—both theoretical and experimental—of negatively charged and neutral sulfur clusters, focusing on trends in the geometries, multiplet structures, and energy differences. The comparison between theory and experiment (Fig. 11 and Table X) indicates that clusters generated by the source are ring-like up to S₅⁻ and chain-like for S₈⁻ and S₉⁻. S₆⁻ and S₇⁻ can occur in both forms, with source adjustments *a* and *b* favoring rings (low VDE) and chains (higher VDE), respectively. The photoelectron spectra [Figs. 17(a)–17(d)] then provide some of the first direct spectroscopic evidence for the existence of different cluster isomers in the gas phase. The existence of multiple isomers can also be inferred from measurements of reaction kinetics.^{67,68}

The transition from closed to open structures as *n* increases through 6–7 is interesting, since the calculations predict that the most stable isomer is closed for all cluster sizes. Although an unambiguous analysis of the growth processes of the clusters would require careful measurements of the

partial pressures, temperatures, and flow velocities at various points in the source, we now show that energetic stability is not the only criterion for the occurrence of particular structures in a cluster beam.

We note first that similar observations have been made in beams of carbon clusters,⁶⁵ where rapid cooling can result in the production of several isomers that are not necessarily the most stable. For example, most C_{60} clusters have ring and double ring structures, and the cage-like fullerene isomer dominates only if slow annealing is allowed. In S_n^- as well, chain-like growth can occur through the addition of terminal atoms, while closed structures involve more complicated growth patterns. For S_6^- and S_7^- , rings are observed when conditions allow a slower cooling of the plasma and more time for the nuclei to rearrange. There are fewer isomers in the smaller clusters, the time required for structural relaxation is shorter, and only the most stable ring-like structures are observed. If the S_n^- clusters grow as chains, ring formation by bonding between the terminal atoms will be hampered by the negative charge localized on these atoms. The net charge on the anion is crucial, as we have found that all chain structures anneal to a closed form if the additional electron is removed.

The isomer distribution in the anions leaving the source is the result of growth, fragmentation, and charge transfer processes. The observation of chain-like isomers is consistent with their higher EA values, since such particles are more likely to survive these processes and be more abundant in the mass spectra. This does not exclude clusters with lower EA, as we have seen in S_6^- and S_7^- . It is possible that ring-like structures could be generated if the cluster beam is annealed suitably, as found in C_n clusters.⁶⁵

We conclude with the observation that the number of chain isomers in the larger clusters is much greater than the number of isomers with closed structures. This can be appreciated by examining the pattern of the signs of the dihedral angles in the structures ("motif").⁶⁹ Closed structures require distinct patterns (such as $+-+ - + - + -$ in the most stable isomer of S_8^-), while open structures can have a variety of combinations of $+$, $-$, and 0 , since the beginning and the end of the chain are not constrained to coincide. The higher configurational freedom of the chains means that they are favored by entropy considerations at higher temperatures, an effect also found in carbon clusters.^{70,71}

The cluster source used in the present study has been applied to transition and noble metals, to alkali metals, and to aluminum and gallium clusters, the last of these being generated from the liquid metal. In the present work, the sample is nonmetallic sulfur. Together with detailed theoretical calculations, such as those described here, it should in the future be able to provide information about the structures of clusters of other elements and of molecules containing more than one element.

ACKNOWLEDGMENTS

We thank numerous colleagues for their help in this project, particularly P. Ballone for many discussions and suggestions, P. Margl for providing the program to calculate

vibration frequencies, D. Hohl and P. Margl for help in using it, and W. Eberhardt for support of the experimental program. We thank the German Supercomputer Center (HLRZ) for a grant of CPU time on the Cray YMP8/864 in the Forschungszentrum Jülich.

APPENDIX: HARTREE ENERGY OF AN ISOLATED CLUSTER

We discuss here the details of our energy calculations for charged clusters. Within the DF scheme, we require the Hartree energy of a density of the form

$$n_t(\mathbf{r}) = n(\mathbf{r}) + n_0,$$

where $n(\mathbf{r})$ is the valence electron density

$$n(\mathbf{r}) = \sum_i f_i |\psi_i(\mathbf{r})|^2$$

of the Kohn–Sham states $\psi_i(\mathbf{r})$ with occupation numbers f_i , and n_0 denotes a uniform background charge required for charge neutrality. Since we use large unit cells and a single \mathbf{k} point, there is no integration over the Brillouin zone. It is convenient to evaluate the Hartree energy in \mathbf{k} space using the fast Fourier transform (FFT) technique

$$\frac{1}{2} \int_{\Omega} d\mathbf{r} \int d\mathbf{r}' \frac{n_t(\mathbf{r})n_t(\mathbf{r}')}{|\mathbf{r}-\mathbf{r}'|} = \frac{1}{2} \sum'_{\{\mathbf{G}_k\}} \Omega \left| \frac{n(\mathbf{G}_k)}{N} \right|^2 \frac{4\pi}{G_k^2}.$$

Here, Ω denotes the volume of the unit cell of the periodic lattice. The only contribution of n_0 is to eliminate $\mathbf{G}_k=0$, which is then excluded from the sum (indicated by the prime). $\{\mathbf{G}_k\}$ denotes the set of reciprocal FFT lattice vectors:

$$\mathbf{G}_k = \sum_{i=1}^3 k_i \mathbf{b}_i, \quad k_i = -\frac{N_i}{2} + 1, \dots, \frac{N_i}{2}$$

conjugate to the real-space FFT mesh

$$\mathbf{r}_j = \sum_{i=1}^3 j_i \frac{\mathbf{a}_i}{N_i}, \quad j_i = 0, \dots, N_i - 1$$

of size $N_1 N_2 N_3 =: N$ within the unit cell containing the cluster (\mathbf{a}_i denote the primitive basis vectors, \mathbf{b}_i denote the basis vectors of the reciprocal lattice, and the N_i are assumed to be even for simplicity).

The essential step in our procedure amounts to a rigid separation of the clusters and their electronic densities as determined in the original unit cells, by distances $l|\mathbf{a}_i|$ in each direction of the direct lattice, while maintaining periodicity. The uniform background charge in the space between the clusters is accordingly reduced to n_0/l^3 . In \mathbf{k} space, this is accompanied by an expansion of the real-space FFT mesh to

$$\mathbf{r}'_{j'} = \sum_{i=1}^3 j'_i \frac{\mathbf{a}_i}{N_i}, \quad j'_i = 0, \dots, lN_i - 1$$

of size l^3N and a refinement of the conjugate \mathbf{k} space mesh to

$$\mathbf{G}_{\mathbf{k}'} = \sum_{i=1}^3 k'_i \frac{\mathbf{b}_i}{l}, \quad k'_i = -\frac{lN_i}{2} + 1, \dots, \frac{lN_i}{2}.$$

The Coulomb potentials of this sequence of densities converge in the limit of infinite separation of the cells ($l \rightarrow \infty$) to the solution of the Coulomb equation for an isolated cluster cut at the cell boundaries and obeying zero boundary conditions at infinity. That is, $n(\mathbf{r}) = \sum_i f_i |\psi_i(\mathbf{r})|^2$, if \mathbf{r} is in the original unit cell and $n(\mathbf{r}) = 0$ otherwise.

It is possible to reduce the computational effort substantially, since we need only the FFT components of the density $n(\mathbf{r})$ that is continued to the larger mesh by the prescription $n(\mathbf{r}_j) = 0$, $\mathbf{r}_j \notin \Omega$. We note that each vector of the finer \mathbf{k} space mesh can be decomposed unambiguously into a sum of a vector $\mathbf{G}_{\mathbf{k}}$ of the coarser mesh and a vector $\boldsymbol{\gamma}_{\mathbf{k}''}$:

$$\mathbf{G}_{\mathbf{k}'} = \mathbf{G}_{\mathbf{k}} + \boldsymbol{\gamma}_{\mathbf{k}''}, \quad \boldsymbol{\gamma}_{\mathbf{k}''} = \sum_{i=1}^3 k''_i \frac{\mathbf{b}_i}{l}, \quad k''_i = 0, \dots, l-1.$$

The set $\{\boldsymbol{\gamma}_{\mathbf{k}''}\}$ contains l^3 vectors. The FFT components on this mesh can be written as

$$\begin{aligned} n_c(\mathbf{G}_{\mathbf{k}'}) &= n_c(\mathbf{G}_{\mathbf{k}} + \boldsymbol{\gamma}_{\mathbf{k}''}) \\ &= \sum_{\mathbf{r}_j} n_c(\mathbf{r}_j) \exp -i(\mathbf{G}_{\mathbf{k}} + \boldsymbol{\gamma}_{\mathbf{k}''})\mathbf{r}_j \\ &= \sum_{\mathbf{r}_j} [n_c(\mathbf{r}_j) \exp -i\boldsymbol{\gamma}_{\mathbf{k}''}\mathbf{r}_j] \exp -i\mathbf{G}_{\mathbf{k}}\mathbf{r}_j, \end{aligned} \quad (\text{A1})$$

so that we need l^3 FFTs, each of length N , to compute the l^3N FFT components of the entire set $\{\mathbf{G}_{\mathbf{k}'}\}$. The number of operations for a single FFT is of the order $l^3N \log_2(l^3N)$, while the present procedure needs $l^3N \log_2(2N) - N$ operations [including $(l^3 - 1)N$ operations to compute the quantities in the brackets in Eq. (A1)]. As usual in this context, "operation" means a complex multiplication that is followed optionally by a complex addition. In the present case, this leads to a reduction in the number of operations by about 50% on average.

In the present work, we calculate the FFT components and Hartree energies for several $l_1 \leq l_2 \leq \dots$ and extrapolate polynomially to the limit $l \rightarrow \infty$. By taking $l_n = 2l_{n-1}$, one can use all the components of the previous steps, since $\{\mathbf{G}_{\mathbf{k}'}\}_{l_{n-1}} \subset \{\mathbf{G}_{\mathbf{k}'}\}_{l_n}$. We have used $l_{\max} = 8$ in the results presented in this paper.

¹J. Donohue, *The Structure of the Elements* (Wiley, New York, 1974), Chap. 9.

²T.P. Martin, *J. Chem. Phys.* **81**, 4427 (1984).

³P. Lenain, E. Picquenard, J. Corset, D. Jensen, and R. Stuedel, *Ber. Bunsenges. Phys. Chem.* **92**, 859 (1988).

⁴G.D. Brabson, Z. Mielke, and L. Andrews, *J. Phys. Chem.* **95**, 79 (1991); P. Hassanzadeh and L. Andrews, *ibid.* **96**, 6579 (1992).

⁵See J.H. Lunsford and D.P. Johnson, *J. Chem. Phys.* **58**, 2079 (1973), and references therein.

⁶H. Hotop and W.C. Lineberger, *J. Phys. Chem. Ref. Data* **14**, 731 (1985).

⁷R.J. Celotta, R.A. Bennett, and J.L. Hall, *J. Phys. Chem.* **60**, 1740 (1974).

⁸N.R. Nimlos and G.B. Ellison, *J. Phys. Chem.* **90**, 2574 (1986).

⁹T. Schindler, C. Berg, G. Niedner-Schatteburg, and V.E. Bondybey, *Ber. Bunsenges. Phys. Chem.* **96**, 1114 (1992).

¹⁰S.B. Woo, E.M. Helmy, P.M. Mauk, and A.P. Paszek, *Phys. Rev. A* **24**, 1380 (1981).

¹¹D. Hohl, R.O. Jones, R. Car, and M. Parrinello, *J. Chem. Phys.* **89**, 6823 (1988).

¹²K. Raghavachari, C.McM. Rohlfing, and J.S. Binkley, *J. Chem. Phys.* **93**, 5862 (1990).

¹³G.E. Quelch, H.F. Schaefer, and C.J. Marsden, *J. Am. Chem. Soc.* **112**, 8719 (1990).

¹⁴W. von Niessen, *J. Chem. Phys.* **95**, 8301 (1991).

¹⁵V.G. Zakrzewski and W. von Niessen, *Theor. Chim. Acta* **88**, 75 (1994).

¹⁶R.D. Mead, A.E. Stephens, and W.C. Lineberger, in *Gas Phase Ion Chemistry*, edited by M.T. Bowers (Academic, Orlando, 1984), p. 213, and references therein.

¹⁷For applications to metal clusters, see C.Y. Cha, G. Ganteför, and W. Eberhardt, *J. Chem. Phys.* **99**, 6308 (1993); **100**, 995 (1994).

¹⁸M. Levy, J.P. Perdew, and V. Sahni, *Phys. Rev. A* **30**, 2745 (1984).

¹⁹J. Yi, D.J. Oh, J. Bernholc, and R. Car, *Chem. Phys. Lett.* **175**, 461 (1990).

²⁰G. Bachelet, D.R. Hamann, and M. Schlüter, *Phys. Rev. B* **26**, 4199 (1982).

²¹R.O. Jones and D. Hohl, *Int. J. Quantum Chem., Quantum Chem. Symp.* **24**, 141 (1990).

²²F.H. Stillinger, T.A. Weber, and R.A. LaViolette, *J. Chem. Phys.* **85**, 6460 (1986).

²³W. Klyne and V. Prelog, *Experientia* **16**, 521 (1960).

²⁴M. Lin and J.H. Lunsford, *J. Magn. Reson.* **29**, 151 (1978).

²⁵R. Stuedel, R. Reinhardt, and F. Schuster, *Angew. Chem.* **89**, 756 (1977); *Angew. Chem. Int. Ed. Eng.* **16**, 715 (1977).

²⁶R. Stuedel, J. Steidel, J. Pickardt, F. Schuster, and R. Reinhardt, *Z. Naturforsch. Teil B* **35**, 1378 (1980).

²⁷R. Stuedel, in *Studies in Inorganic Chemistry*, edited by A. Müller and B. Krebs (Elsevier, Amsterdam, 1984), Vol. 5, p. 3.

²⁸R. Stuedel, *Nova Acta Leopoldina* **59**, 231 (1985).

²⁹P. Coppens, Y.W. Yang, R.H. Blessing, W.F. Cooper, and F.K. Larsen, *J. Am. Chem. Soc.* **99**, 760 (1977).

³⁰See, for example, R.O. Jones and O. Gunnarsson, *Rev. Mod. Phys.* **61**, 689 (1989).

³¹R. Stuedel, T. Sandow, and J. Steidel, *Z. Naturforsch. Teil B* **40**, 594 (1985).

³²R. Stuedel, *Angew. Chem.* **87**, 683 (1975); *Angew. Chem. Int. Ed. Eng.* **14**, 655 (1975).

³³R. Stuedel, *Angew. Chem.* **89**, 757 (1977); *Angew. Chem. Int. Ed. Eng.* **16**, 716 (1977).

³⁴R. Stuedel, *Z. Naturforsch. Teil B* **38**, 543 (1983).

³⁵L. Pauling, *Proc. Natl. Acad. Sci.* **34**, 495 (1949).

³⁶W. de Heer, *Rev. Mod. Phys.* **65**, 611 (1993).

³⁷V. Bonačić-Koutecký, P. Fantucci, and J. Koutecký, in *Clusters of Atoms and Molecules*, edited by H. Haberland (Springer, Berlin, 1994), p. 15.

³⁸U. von Barth, *Phys. Rev. A* **20**, 1693 (1979).

³⁹Since the l and m_l quantum numbers of the one-particle orbitals that enter the determinantal states cannot be controlled directly in the LSD approximation, we use instead states that yield the same densities (and energies) as the latter. Since the $3p$ subshell is not closed, the densities of determinantal states of interest are not spherically symmetrical, and a self-consistent computation leads to a splitting of the energies of orbitals with different $|m_l|$. In the case of a p shell, the doubly degenerate orbitals belonging to $|m_l|=1$ can be distinguished from the single level with $|m_l|=0$. Since the contribution to the density does not depend on the sign of m_l , one needs only guarantee that the (spin-) occupation of every $|m_l|$ subspace is the same as in a determinantal case in order to obtain its energy.

⁴⁰The transition energies into some multiplet states, such as the $^1\Sigma_u^-$, $^1\Sigma_u^+$, $^3\Sigma_u^-$, $^3\Sigma_u^+$, $^1\Delta_u$, and $^3\Delta_u$ of the $\dots 5\sigma_g^2 2\pi_u^3 2\pi_g^3$ configurations of S_2^- , cannot be computed with the above fitting procedure. The orbitals in the determinants required differ only in the signs of the magnetic quantum numbers λ and cannot be distinguished within the LSD approximation.

⁴¹For this information, please contact R.O. Jones (internet: r.jones@kfa-juelich.de).

⁴²S. Yang, K.J. Taylor, M.J. Craycraft, J. Conceicao, C.L. Pettiette, O. Cheshnovsky, and R.E. Smalley, *Chem. Phys. Lett.* **144**, 431 (1988).

⁴³G. Delacrétaz, E.R. Grant, R.L. Whetten, L. Wöste, and J.W. Zwanziger, *Phys. Rev. Lett.* **56**, 2598 (1986).

- ⁴⁴E.A. Rohlffing and J.J. Valentini, *Chem. Phys. Lett.* **126**, 113 (1986).
- ⁴⁵P.F. Bernath, K.H. Kinkle, and J.J. Keady, *Science* **244**, 562 (1989).
- ⁴⁶T.N. Kitsopoulos, C.J. Chick, A. Weaver, and D.M. Neumark, *J. Chem. Phys.* **93**, 6108 (1990).
- ⁴⁷K.J. Taylor, C. Jin, J. Conceicao, L.S. Wang, O. Cheshnovsky, B.R. Johnson, P.J. Nordlander, and R.E. Smalley, *J. Chem. Phys.* **93**, 7515 (1990).
- ⁴⁸C.C. Arnold and D.M. Neumark, *J. Chem. Phys.* **99**, 3353 (1993).
- ⁴⁹D.G. Leopold, J.Ho, and W.C. Lineberger, *J. Chem. Phys.* **86**, 1715 (1987).
- ⁵⁰O. Cheshnovsky, S.H. Yang, C.L. Pettiette, M.J. Craycraft, Y. Liu, and R.E. Smalley, *Chem. Phys. Lett.* **138**, 119 (1987).
- ⁵¹P. Margl, K. Schwarz, and P.E. Blöchl, *J. Chem. Phys.* **100**, 8194 (1994).
- ⁵²J. Kohanoff, *Comput. Mater. Sci.* **2**, 221 (1994); J. Kohanoff, W. Andreoni, and M. Parrinello, *Phys. Rev. B* **46**, 4371 (1992).
- ⁵³C.A. Sawicki and D.B. Fitchen, *J. Chem. Phys.* **65**, 4497 (1976).
- ⁵⁴R.J.H. Clark and D.G. Cobbold, *Inorg. Chem.* **17**, 3169 (1978).
- ⁵⁵K.P. Huber and G. Herzberg, *Molecular Spectra and Molecular Structure. IV. Constants of Diatomic Molecules* (Van Nostrand Reinhold, New York, 1979).
- ⁵⁶B. Meyer, T. Stroyer-Hansen, and T.V. Oommen, *J. Mol. Spectrosc.* **42**, 335 (1972).
- ⁵⁷S.-Y. Tang and C.W. Brown, *Inorg. Chem.* **14**, 2856 (1975).
- ⁵⁸A.G. Hopkins, S.Y. Tang, and C.W. Brown, *J. Am. Chem. Soc.* **95**, 3486 (1973).
- ⁵⁹P. Lenain, E. Picquenard, J.L. Lesne, and J. Corset, *J. Mol. Struct.* **142**, 355 (1986).
- ⁶⁰E. Picquenard, O. El Jaroudi, and J. Corset, *J. Raman Spectrosc.* **24**, 11 (1993).
- ⁶¹J.E. Rice, R.D. Amos, N.C. Handy, T.J. Lee, and H.F. Schaefer III, *J. Chem. Phys.* **85**, 963 (1986).
- ⁶²C.W. Murray, N.C. Handy, and R.D. Amos, *J. Chem. Phys.* **98**, 7145 (1993).
- ⁶³C.Y. Cha, G. Ganteför, and W. Eberhardt, *Rev. Sci. Instrum.* **63**, 5661 (1992).
- ⁶⁴G. Ganteför, H.R. Siekmann, H.O. Lutz, and K.H. Meiwes-Broer, *Chem. Phys. Lett.* **165**, 293 (1990); H.R. Siekmann, C. Lüder, J. Faehrmann, H.O. Lutz, and K.H. Meiwes-Broer, *Z. Phys. D* **20**, 417 (1991).
- ⁶⁵H. Handschuh, G. Ganteför, B. Kessler, P.S. Bechthold, and W. Eberhardt, *Phys. Rev. Lett.* **74**, 1095 (1995).
- ⁶⁶C.E. Moore, *Natl. Bur. Stand. (U.S.) Circ. No. 467*, Vol. I (1949), Vol. II (1952), Vol. III (1958).
- ⁶⁷S.W. McElvany, B.I. Dunlap, and A. O'Keefe, *J. Chem. Phys.* **86**, 715 (1987).
- ⁶⁸See, for example, K.M. Creegan and M.F. Jarrold, *J. Am. Chem. Soc.* **112**, 3768 (1990), and references therein.
- ⁶⁹F. Tuinstra, *Structural Aspects of the Allotropy of Sulfur and Other Divalent Elements* (Waltman, Delft, 1967).
- ⁷⁰D.E. Bernholdt, D.H. Magers, and R.J. Bartlett, *J. Chem. Phys.* **89**, 3612 (1988) [C_4].
- ⁷¹W. Andreoni, D. Scharf, and P. Giannozzi, *Chem. Phys. Lett.* **173**, 449 (1990) [C_4 , C_{10}].
- ⁷²R. Steudel, *Spectrochim. Acta Part A* **31**, 1065 (1975).